Biotechnology Reports 44 (2024) e00860

Contents lists available at ScienceDirect

Biotechnology Reports

journal homepage: www.elsevier.com/locate/btre

Review

Agrowaste-carbon and carbon-based nanocomposites for endocrine disruptive cationic dyes removal: A critical review

Adewumi O. Dada [a,b,f,g,h,*], Adejumoke A. Inyinbor [a,f], Bukola T. Atunwa [a,f], Spandana Gonuguntla [b,e], Olugbenga S. Bello [c,f], Folahan A. Adekola [d], Ujjwal Pal [b,e]

[a] Industrial Chemistry Programme, Nanotechnology Laboratory, Department of Physical Sciences, Landmark University, P.M.B.1001, Omu-Aran, Kwara, Nigeria
[b] Department of Energy and Environmental Engineering, CSIR-Indian Institute of, Chemical Technology, Hyderabad, India
[c] Department of Pure and Applied Chemistry, Ladoke Akintola University of Technology, Ogbomoso, Nigeria
[d] Department of Industrial Chemistry, P.M.B 1515, University of Ilorin, Ilorin, Nigeria
[e] Academy of Scientific and Innovative Research (AcSIR), Ghaziabad-201002, India
[f] Sustainable Development Goal 6: Clean Water and Sanitation, Landmark University, P.M.B.1001, Omu-Aran, Kwara, Nigeria
[g] Sustainable Development Goal 7: Affordable and Clean Energy, Landmark University, P.M.B.1001, Omu-Aran, Kwara, Nigeria
[h] Sustainable Development Goal 11: Sustainable Cities and Communities, Landmark University, P.M.B.1001, Omu-Aran, Kwara, Nigeria

ARTICLE INFO

Keywords:
Cationic dyes
Agro-residue carbon
Nanocomposites
Adsorption
Isotherm and kinetics and thermodynamics

ABSTRACT

Dyes are considered to be pollutants that pose a considerable worldwide health risk, as they have been discovered as agents that affect the endocrine system. Adsorption is the most commonly used method for removing different substances since it is sustainable, flexible, affordable, and easy to use. Researchers have investigated the usage of agro-waste-based adsorbents that are ecologically friendly for the process of adsorption. This research has emphasized the potential of these adsorbents in developing carbon-based nanocomposites. Improved surface functionalization, great compatibility, and flexibility are beneficial uniqueness of carbon-based nanocomposites as well as a wide variety of applications. As a result, they are highly successful in removing cationic dyes. This paper specifically examines the environmentally friendly usage of activated carbons obtained from agricultural waste and the development of carbon-based-nanocomposites to adsorb positively charged dyes. Additionally, it offers an in-depth investigation of various cationic dyes, operating parameters, adsorption isotherms, kinetics, processes, and thermodynamic investigations. Further research is necessary to determine the effectiveness of carbon-based nanocomposites in removing new endocrine-disrupting pollutants. Additionally, these nanocomposites have the potential to be widely used in treating industrial effluents.

1. Introduction

With the prevalence of rapid industrialization, and the increase in the use of dyes in different human activities that the world at large has experienced and may keep experiencing, the release of high levels of pollutants into the environment is inevitable. This level of pollution can serve as a threat to both humans as well as plants. Notably, a major source of pollution is the contamination of waterbody with highly toxic pollutants emanating from industries such as textile/clothing [1], pharmaceuticals [2,3], rubber/plastics [4], pesticides, insecticides, metallurgy, and construction industries [5,6] as well as municipal wastewater, amongst others [7]. These pollutants can cause dangerous health hazards to the liver, brain, reproductive organs, etc. Based on past studies, the world has reached 650,000 tons of dyes production and as such, and the presence of 100,000 dyes in commerce [8]. Dyes are estimated to be supplied in millions of tons per year, with 10–15 percent of this amount being discharged into the wastewater, making them significant water pollutants [4]. When dyes are released into an aquatic environment, they produce vividly coloured dye pollutants that are harmful to the ecosystem. Dyes have detrimental impacts on water resources by impeding sunlight penetration, disrupting photosynthetic chain reactions, and compromising the well-being of aquatic species. Most dye molecules consist of aromatic rings, rendering them extremely poisonous and non-degradable [9]. Dyes are extremely hazardous being carcinogenic and have a link to environmental deterioration as well as a variety of ailments in both animals and people [8,10]. Dye molecules in

* Corresponding author.
E-mail address: dada.oluwasogo@lmu.edu.ng (A.O. Dada).

https://doi.org/10.1016/j.btre.2024.e00860
Received 8 April 2024; Received in revised form 9 September 2024; Accepted 13 September 2024
Available online 15 September 2024
2215-017X/© 2024 The Author(s). Published by Elsevier B.V. This is an open access article under the CC BY-NC-ND license (http://creativecommons.org/licenses/by-nc-nd/4.0/).

water could lead to health issues such as kidney dysfunction, liver and brain damage, cancer, and reproductive problems, amongst others. in humans, as well as the disruption of photosynthetic activities in plants. Textile dyes are often categorized into two groups: ionic (which includes anionic and cationic dyes) and non-ionic (specifically dispersed dyes) [7].

Among these dyes, cationic dyes have been known to cause health hazards such as vomiting, irregular heartbeats, jaundice, tissue death (necrosis), cancer of the bladder, and so on [10,11]. Hence, it becomes imperative to clean up these pollutants from wastewater purposely to generally foster access to clean water for all. Cheaper methods for treating wastewater will be far more appreciated as conventional treatment methods of wastewater are considered expensive [12].

Several methods such as oxidation, coagulation, membrane separation process, electrochemical, aerobic, nano-filtration, sedimentation, carbon nanotubes, ozonation, ultrafiltration, anaerobic, aerobic, adsorption [7,9,13,14] etc. have been used to sequestrate these cationic dyes [15,16]. However, these methods are either highly costly, time-consuming, or not so effective. Most often, they are not always easy to operate. They could also lead to the production of hazardous sludge and expensive operational and maintenance expenses [4,17]. In addition, it has been shown that biological techniques used to remove cationic dyes from wastewater, despite being used in several countries, are incapable of achieving total removal [18]. Adsorption has proven over the years to be a much better method for dye pollutant removal. Adsorption is known to be cost-effective and easy to operate. Therefore, the sequestration or removal of cationic dyes by employing the adsorption technique will be discussed in this review. Furthermore, commercial activated carbon (CAC) has been gaining preference over the years owing to its high porosity and large surface area. However, due to the high cost of importing CAC and its complications in re-usability processes, activated carbon produced from agricultural wastes has been employed by several researchers instead of CAC. Currently, numerous researchers are seeking adsorbents composed of metal nanoparticles combined with biodegradable polymer compounds that possess a high adsorption capacity and are cost-effective. Noteworthily, conventional adsorbents such polymeric polymers, coal, silica, and activated carbon have been employed for the purpose of adsorbing dye molecules [16]. For the purpose of this study, we are reporting the use of agro-based activated carbons for cationic dye removal.

These agro-based activated carbons are eco-friendly, easily obtained, reusable, renewability characteristic, economical, chemical composition, excellent efficient, and highly carbonaceous. Moreover, incorporating nanoparticles into agro-based activated carbons could further enhance its applicability in the effective adsorption of endocrine disruptive cationic dye. The review further entails the application of carbon-based nanocomposites for efficient cationic dye removal, various characterization techniques, nitty-gritty in techniques of adsorption, and comparison of the adsorption capacities of previous studies as well as insight into isotherm, kinetics, and thermodynamics of the removal of cationic dyes. Moreover, the efficacy of the carbon-based nanocomposites for cationic dye removal was explored. Therefore, this review will dwell on the adsorption of cationic dyes using low-cost adsorbents produced from agro-residues for wastewater treatment.

1.1. *Sustainable source of low-cost activated carbon*

The sustainable source of low-cost and efficient activated carbon is from agrowastes and they are often referred to as agro-residues. Agro-residues are unwanted wastes that are gotten from agricultural operations or activities. They mainly consist of the following three components: lignin, hemicellulose, and cellulose [19]. Presented in Fig. 1 are various examples of agro-residues and some of them are; cocoa pods [20], orange peels [21,22], cashew nut shells [23,24], bamboo [5, 25–27], durian seeds, coconut coir and shells [28–30], potatoes [31], yam and plantain peels [32,33], watermelon, *Raphia hookeri* [34], rice hulls [35,36], rice bran [37], maize cobs [38–40], sugarcane bagasse [41,42], amongst others. Ultimately, sustainable and low-cost activated carbon could be produced from these sources. The need for an alternative to commercial activated carbon (CAC) stems from the high cost of CAC which is becoming unaffordable to middle and low-income countries. Moreover, the limitation of CAC in terms of regeneration or reusability is also becoming a draw-back [15,43]. To solve these existing issues, agro-residues (carbon-rich agrowaste materials) can be utilized suitable for adsorbent production by the pyrolysis of wastes under oxygen-limited conditions [44,45]. Often, agricultural wastes could litter and disrupt the normal atmospheric conditions in the environment. Hence, an optional way of reducing the environmental pollution caused by these agricultural wastes is to transform them to activated carbon which could be used for nanocomposite development and applied for waste-water treatment in the long-term. Some of the agrowastes employed by researchers are; rice husk, banana stalk and peels [46–48],

Fig. 1. Selected low-cost and environmentally benign agro-residues from different sources.

coconut husk [29,49–51], oil palm [52,53], rice straw [37,54,55], oil palm shell [52,56], sawdust [52], corn cob [6,57,58].

1.2. General activated carbon preparation procedural steps and techniques

Commercial activated carbon (CAC) has been employed in many wastewater clean-up processes, in several sectors of the country. However, agro-residues especially those with high carbonaceous content could be utilized to replace CAC [59]. These agro-residues when used in their raw state may not be as effective as activated carbon, but when they are treated either chemically or physically, their usefulness and effectiveness are highly enhanced due to improved physicochemical and spectroscopic properties. To improve the physicochemical properties of a prepared or synthesized carbon material, the modification of the material has to be done in a well-targeted manner (such as the employment of physical activation or chemical activation [60–63].

Usually, carbonization of the agro-residue is the first step, after which chemical or physical activation is done. The process begins with sample collection after which the sample is washed until it is clean. It could also be cut into smaller sizes, washed and sun-dried or oven-dried at a temperature of 105 °C. It could further be grounded to a fine powder to reduce the particle size. Carbonization is done by transferring the finely washed, dried, and ground agro-wastes into the furnace at a temperature desired. In order to produce effective activated carbon, carbonization is accomplished via pyrolysis/gasification at a higher temperature in an inert environment, leading to a residue that is mainly carbon. The fundamental porous framework of the precursor material is generated by managing carbon burn-off, and the non-graphitic carbon material is essentially gasified, leaving a highly permeable network of highly disorganized graphitic material containing surface oxide groups.

In physical activation, the use of hot gases or steams is usually employed. Most times, chemical activation is preferred over physical activation, because it yields a higher quantity of the sample at the end product as opposed to physical activation. Also, chemical activation requires lower temperatures than physical activation [64,65]. It is noteworthy to also point out that the activated carbon produced as a result of chemical activation, has a higher surface area and porous nature than the ones produced by physical activation. Temperature is a very important parameter during carbonization. Hence, the right temperature should be applied, to get optimum results. Also, pyrolysis in the absence of air is important. Tube furnaces using argon gas is encouraged. Some adsorbents do well at lower pyrolysis temperature, while some do excellently well, at higher pyrolysis temperature. In the study by Adekanye et al. (2022), the temperature for the carbonization of the raw agro-waste varied between 300 °C and 500 °C, in a muffle furnace. The SEM image of the maize cob biochar carbonized at 500 °C showed excellent porous structures as opposed to the maize cob carbonized at 300 °C [66]. The study demonstrated the importance of the temperature used for the physical activation of the maize cob. The study reported a maximum total fixed carbon of the produced adsorbent as 60.5 %, though at 300 °C. While muffle furnace is characterized by uniform heating (i.e., even and consistent heating), versatility, ease of operation, and cost-effectiveness, it has some disadvantages such as limited control over atmosphere inside the muffle furnace chamber and unsuitable for some particular and precise pyrolysis processes. Tube furnace on the order hand prevent loss of carbon content, offers better atmosphere (e.g., inert gas, vacuum) control in the furnace chamber, which fosters the prevention of oxidation and other reactions. It is also advantageous as itis more precise and it encourages the specific configurations which are also useful for continuous processes. Tube furnace also minimizes sample weight loss better than a muffle furnace, due to its superior control abilities (precise temperature regulation and better controlled atmosphere). A main disadvantage is that its more costly than muffle furnaces and it has sample size constraints. The size of the sample could therefore be reduced to smaller sizes to foster easier input into the tube furnace.

Generally, the sample size and characteristics, cost, ease of use, nature of the pyrolysis process (in terms of atmosphere and temperature control) and, sample weight loss, must be considered before decisions are made on which type of furnace you may want to use in a research study.

In the chemical activation process, before heating begins, the activation agent to be employed, such as H_3PO_4 or $ZnCl_2$, will be incorporated into the biochar. Some other chemicals utilized for chemical activation are HCl, (H_2SO_4), NaOH, and H_2O_2. The beaker containing both the activating agent and biochar is heated until a slurry forms. The slurry formed will then be transferred into labelled crucibles and placed in a furnace (at the chosen temperature and for a determined period) to complete the activation process. The activated carbon sample can later be brought out of the furnace (after the set time) or microwaved and left to cool down slowly, after which it can then be washed till the pH of the sample is neutral. Immediately after washing, it should be oven-dried at 105 °C and further kept in an airtight container for further use [67–70].

Often, after activation, there would be either broadening of identified peaks in the raw sample or even disappearances and appearances of some new peaks. These peaks can be identified by Fourier Transmittance Infrared analysis. An example of this can be observed from the study by Bello et al. (2021), who acidified the raw mango pod and the FTIR results of the acidified mango pod showed appearances and disappearances of some functional peaks [71]. According to another study, there was an increase in the pore diameter of the chemically manufactured activated carbon sample, after activation was done [33]. Plantain peels agro-wastes was washed and sundried in a study by Dada et al., 2021. The carbonization/pyrolysis of the plantain peel was done at 400 °C for 1 h, while chemical activation was carried out at 400 °C for 1 h after the carbonization process was completed. The resulting activated sample, prove to be efficient for the adsorption of chloroquine. Importantly, parameters such as temperature, heating duration as well as time required for carbonization should be carefully noted, because they can affect the end product of the carbonization process [72,73]. This section summarizes the different agrowaste sources and their physical and chemical processes involved in making it an effective activated carbon that can be used in place of commercial activated carbon.

2. Nanoparticles and carbon-supported nanocomposites

The word nano refers to particles as small as one-billionth or 10^{-9} and when considering 1 nm, it has a measurement equal to 10^{-9} metres [74,75]. A rich interest in nanoparticles is on the rise among researchers based on their wide applications arising from their unique properties and characteristics and also serving as a link between massive and bulk materials. For instance, zinc oxide nanoparticles had already been proven to possess greater UV-blocking qualities when compared to their bulk form, which is among the justifications for their frequent use in the creation of sunscreen creams, coupled with the fact that they are very photostable [1,76,77]. When materials are brought together and combined, they form what is known as a composite. Interestingly, the resulting composite, formed through the combination of individual materials, exhibits enhanced strength compared to its constituent components. Nanocomposites, distinguished by their nano-scale dimensions, are comprised of various nanomaterials. These nanomaterials may be soft, or a mixture of both hard and soft types. The properties of synthesized nanocomposites are influenced by the morphology of the nanomaterials, the characteristics of their interfaces, and the inherent nature of the individual materials used in the combination [78]. Each of these materials will be combined in such a way that their physical phases remain intact. These materials must not be soluble in each other and must not form any new chemical compound. This explains why a nanocomposite is often referred to as a material system that is multi-phased by other researchers [79,80]. The advantages of adding these nanocomposites include properties such as strength, toughness

and electrical or thermal conductivity, etc. [81]. It is highly possible to change the basic characteristics of materials, such as the melting temperature, the magnetic properties, the charge capacity of the material, and also colour, without affecting their chemical components, by building nanometer-scale frameworks [81]. Nanocomposites are better alternatives to the use of monolithic and micro composites [82].

Agro-based nanocomposites are employed by different researchers as efficient absorbents for wastewater treatment in the adsorption of water pollutants as relevant to separation science. Agro-based nanocomposites are made of agricultural wastes and other nano-materials. Oftentimes, when agro-residues are loaded onto nanoparticles, they improve the porosity as well as the adsorption efficiency of the nanoparticles. A study in 2018, adsorbed methylene blue using agro-residue-derived carbons [83]. The nanocomposites (AgNP-PKSAC) employed in another study, were obtained from the combination of palm kernel shells and silver nanoparticles. The agro-residues used, served as a support for silver nanoparticles synthesized. The study reported that the agro-residues improved the porosity of the adsorbent and improved their usability as catalysts. Most often, the selection of the best method for the synthesis of the nanocomposites that can be used to remove cationic dyes is based on the type of catalyst to be used, the base material to be incorporated and the type and nature of contaminants or pollutants to be degraded or adsorbed [84].

2.1. Techniques of nanocomposite development

Nanocomposite development is based on techniques among which are: the hydrothermal technique, electrospinning technique, sol-gel method, impregnation technique, pulse laser ablation, ion-exchange technique, microwave, ion-sputtering scattering, template synthesis, spark discharge, and precipitation technique [72,85–89]. Hydrothermal and solvothermal preparation techniques are used for the development of nanomaterials that are characterized by diverse morphological properties. The hydrothermal method involves mixing the metal catalyst and other supporting reactants in the water in a heated, sealed, and Teflon-lined autoclave [90,91]. However, when an organic solvent is used instead of water, the method or technique used is referred to as solvothermal. In the sol-gel method, instruments that are not too complex and are easy to operate with are used. Also, the sol-gel method does not require extreme temperatures or high pressures [45]. The method is characterized by the ability to be tailored over textural properties and the base materials play a big role. The electrospinning technique is used to develop continuous nano-fibres which are characterized by diameters that are ten nanometres to micrometres. Precipitation and co-precipitation are used for the concurrent precipitation of two or more components. This technique is characterized by the ability to produce particles that have different sizes. In co-precipitation, nucleation, growth, agglomeration, and coarsening take place simultaneously [92]. Different characteristics shown or exhibited by the method include the development of insoluble species developed under very high supersaturated circumstances and the development of large small particles. A flow chart of the formation of nanocomposite is presented in Fig. 2.

In the preparation of the TiO_2/Fe_2O_3 nanostructures as reported by a previous study, the sol-gel method was employed. The nanostructures produced had high stability, as they were re-used four times. They also showed high degradation efficiency as reported in a previous study, as such can be projected for even bigger projects [93]. Also, a bottom-up approach was employed in the creation of silver nanoparticles (AgNPs) in 2019. A medicinal plant extract obtained from *Acalypha wilkesiana* (AW) was used for synthesizing silver nanoparticles too. The result was the production of an exceptional adsorbent, referred to as AW-AgNPs. FTIR analysis established the occurrence of some functional groups. The reduction of Ag^+ was well confirmed using scanning electron microscopy (SEM) and transmission electron microscopy (TEM). The results showed the spherical shape of well-dispersed AW-AgNPs. The elemental distribution was revealed by EDX. AgNPs were confirmed with a distinctive intense peak at 3.0 keV. The nanoparticles produced (AW-AgNPs) were reported to show noteworthy inhibition against the chosen prevailing bacteria [94]. Various techniques previously applied have been summarized in Table 1. Presented on Table 2 are the agro-wastes materials used as based material for the preparation of activated carbon, the method of nanocomposite development as well as the types of nanocomposites developed. This section encompasses Nanoparticles and Carbon-Supported Nanocomposites and the different techniques of synthesizing them.

3. Characterization

Adsorption research requires numerous critical characterisation approaches to confirm and validate activated carbons and nanocomposites' superior characteristics. Thus, this section explains more on these approaches/tests used in an adsorption study. FTIR detects surface functional groups, essential for dye molecule chemical interactions. XRD examines crystalline structure to reveal adsorption-affecting structural changes. EDX analyses elemental composition for dopants and impurities. SEM and TEM show texture, porosity, and nanoparticle distribution by examining surface appearance and interior structure. Higher surface areas provide superior adsorption capabilities, according to Brunauer-Emmett-Teller (BET) surface area study. TGA measures thermal stability and composition, whereas zeta potential analysis measures surface charge under different pH levels to anticipate adsorbent-dye electrostatic interactions. These methods reveal the physical, chemical, and structural factors that affect adsorption effectiveness [114,115].

3.1. Fourier transform infrared (FTIR)

The Fourier transform Infrared is one of the analyses that needs to be done during characterization in order to identify the chemical environment in terms of functional groups present in a sample within the

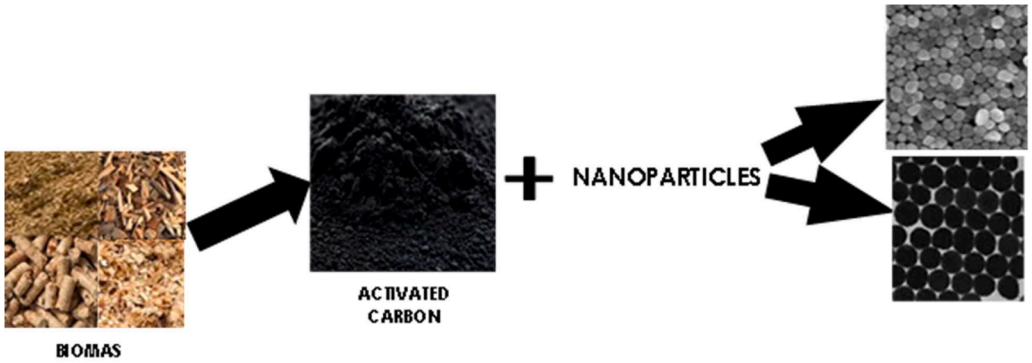

Fig. 2. A flowchart showing the pictorial and morphological representation of the development of carbon-based-nanocomposites from biomass.

Table 1
Different carbon-based nanocomposites and their methods of preparation.

Agro-material	Method of preparation	Type of Nanocomposites Developed	Dimension/size/shape of nanoparticles	References
Orange peel	Microwave-assisted	CQDs combined with magnetic nanoparticles	4.20 nm (spherical)	[95]
Oil palm bagasse	Sol-gel method	Oil palm-Al_2O_3 nanoparticles	58.56–12.64 nm	[96]
Papaya peel extract	Sol-gel method	CuO nanoparticles	85–140 nm, Agglomerated spherical	[97]
Citrus peel	One-pot hydrothermal approach co-precipitation method	Bio-nano-composite (MGDCP)	490 nm, spherical-shaped	[98]
Rice husk	A modified chemical co-precipitation method	Magnetic biochar	10–14 nm spherical and uniform shape	[55]
Orange peel	Precipitation	Iron nanoparticles	tabular structure (20 nm), octahedral shape (20–40 nm)	[99]
Coconut shell	Sol-gel method	TiO_2/BC composites	490 nm spherical-shaped and monodisperse	[100]
Banana peel waste	Hydrothermal method	Carbon quantum dots (CQDs)	5 nm, spherical	[91]
Coconut shell	Direct precipitation method	ZnO nanoparticles	20 nm, pseudo-spherical shape	[101]
Orange peel	Sol-gel method	TiO_2 and Al_2O_3 nanoparticles	19.13 nm	[102]
Coconut shell	Precipitation method	CuO—Nanoporous activated carbon	40–70 nm, spherical in shape	[24]
Orange peel	Hydrothermal	Fe-modified hydrochar		[97]
Orange fruit peel	Precipitation method	ZnO nanoparticles	39.70 nm spherical-like shape	[103]
Coconut shell	Co-precipitation	Activated carbon–iron oxide composite	–	[104]
Shrimp shells	Sol-gel	Fe/ZnO-shrimp shell nanocomposites	–	[105]
Coconut shell	Co-precipitation	AB-MnO_2 nanocomposites	symmetric triangular-like shape	[106]
Coconut shell	Co-precipitation	Magnetic-activated carbon and magnetic biochar	0.20- 2.70 nm	[107]
Coconut shell	Hydrothermal	CSAC-ZnO at various temperatures (400, 600 and 800 °C)	17.33–56.48 nm, hexagonal shape	[108]

Table 2
Types, advantages and disadvantages of cationic dye method of removal.

Methods Categorization	Types	Advantages	Disadvantages	Reference
Chemical	Coagulation; ozonation; oxidative processes; electrocoagulation; ion exchange; Fenton reactions, electrochemical oxidation, etc.	Low cost; effective in decolourizing dyes; the end products in the process are not hazardous when employing the electrochemical destruction method; simplicity.	The half-life of the products when the ozonation method is employed is usually small; employing electrochemical destruction methods could be costly due to electricity and the cost of operation.	[109–111]
Biological	Adsorption using microbial biomass as the adsorbent; nitrification; using fungicides in a bleaching process; using activated sludge tanks; bioremediation, etc.	Biogas production; decolourization of azo and anthraquinone dyes. The sludge treatment procedure takes place at a pH of neutral.	Low colour removal rates; necessarily involve particular oxygen-catalyzed enzymes; and necessitate extra carbon and power sources; it could also require a unique bioreactor as well as an exterior carbon supply.	[110–112]
Physical	Nanofiltration; irradiation; activated carbon, use of other agricultural and industrial by-products; adsorption; ultrafiltration and microfiltration; ion exchange.	Suitable for removing many cationic dyes; relatively inexpensive; adsorbents used could be very effective; simplicity of design process;	The ion exchange method is not effective in removing some dyes; the surface area of some adsorbents could be low; the filtration methods may not be able to treat large volumes.	[112,113]

range of 4000–400 cm^{-1}. FTIR aids in the identification of the surface functional groups and understanding the mechanism, and nature of the properties of the surface of the carbon adsorbent and carbon-based nanocomposites. This is usually done by scanning the chosen organic, inorganic or polymeric samples of interest with infrared light [16,33,116,117]. In most cases, the functional groups of the samples before and after adsorption are determined. The common functional groups such as; – OH, -C = C-, - C – O are generally reported in several adsorption studies involving carbon-activated and carbon-based nanocomposites [10,118]. The FTIR results of the maize cob biochar of our previous studies as seen in Fig. 3a, where maize cob char produced at 500 °C showed excellent peaks at 3402.54 connoting the presence of O—H stretching (alcohol), other functional groups present include C = C, C—H, C—O [66,119]. In past research by Dada et al. (2021), the agro-waste used as the precursor was plantain peel. Activation of the plantain peel was done using H_3PO_4, and peaks observed revealed the presence of O—H, C—O, and C—H stretch functional groups. The activated carbon produced in that study was incorporated with ZnO nanoparticles producing carbon-based nanocomposites [33]. The FTIR analysis of activated carbon after adsorption of cationic dyes always resulted in a shift of bands, disappearance of peaks, and collapses of bonds [120,121]. Also, in carbon-nanocomposites, researchers have always observed the interaction of the carbon samples with nanoparticles thereby causing a shift of bands [122–124]. The FTIR results of zinc chloride-activated ackee apple pods (ZACAPP) showed the presence of the important peaks that help us understand if the sample contains the needed functional groups that help in determining its relevance and effectiveness as seen in Fig. 3c & 3d.

3.2. X-ray diffraction (XRD) and energy dispersive X-ray (EDX)

X-ray diffraction (XRD) helps in understanding the crystallinity and nature of the sample being analyzed, while the EDX provides information on the elemental identification of elements present or absent in a given material. The XRD studies in Figs. 4(a-c) showed changes in the crystallinity of the nanoparticles and carbon-based nanocomposite and mostly the amorphous nature of the carbon as based material and electron sink could be identified using XRD [126]. The XRD pattern of Fe (0)-FeS and CNF@Fe(0)-FeS were shown in Fig. 4(a). Peaks at 62.9° and 60° were matched to (023) and (222). The XRD study attested that CNF@Fe(0)-FeS consisted of Fe(0) as well as FeS [76]. The XRD pattern of palm kernel shell-activated carbon and PKSAC-AgNPs showed a broad amorphous nature due to the presence of the carbon. The peaks at 64.77°, 44.66° as well as 38.21° in Fig. 4b, revealed a peak that is

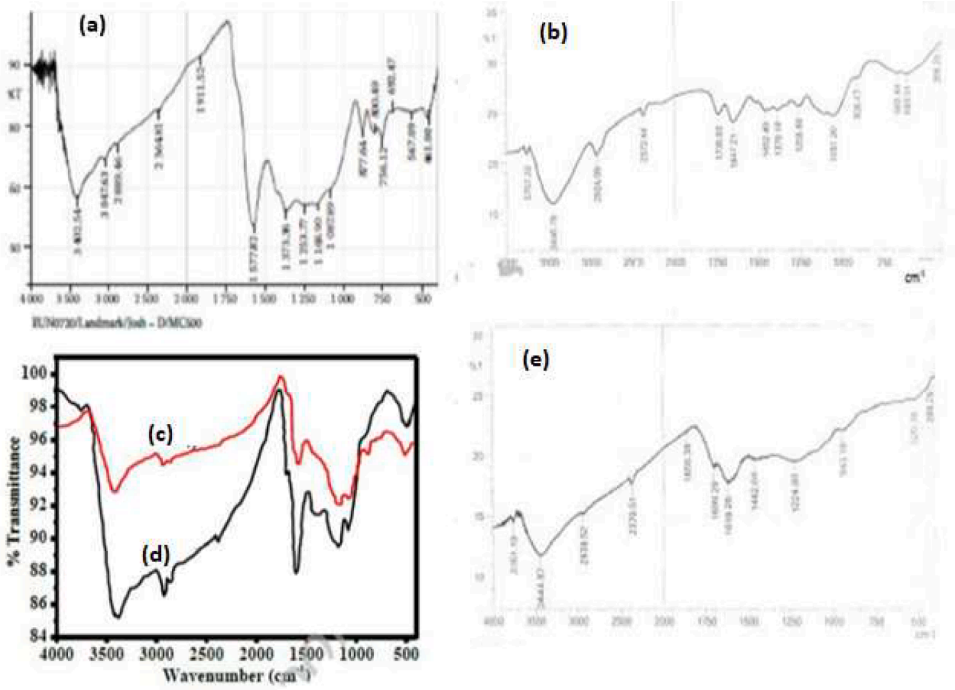

Fig. 3. (a-e): FTIR spectrum of maize cob biochar produced at 500 °C, Moringa seed pod raw (MOSPR), Zinc-activated carbon of ackee apple pod at 400 °C and 500 °C respectively and Moringa seed pod activated carbon (MOSPAC) [66,120,125].

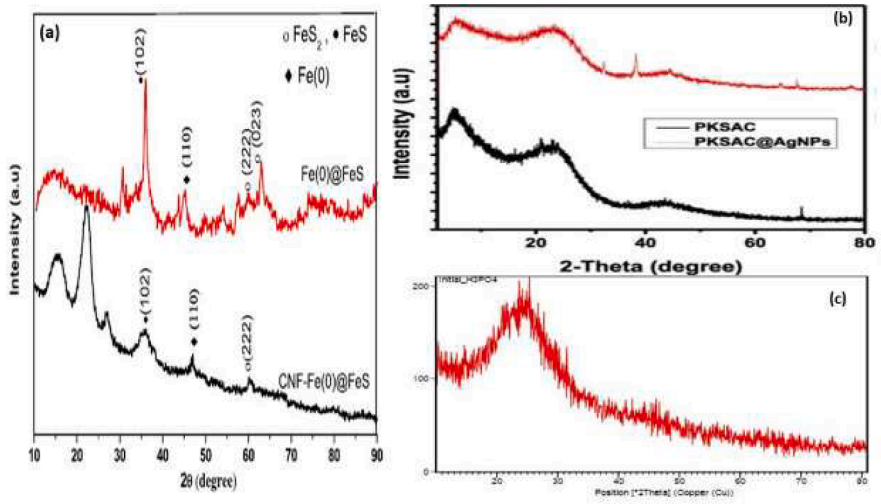

Fig. 4. (a-c): XRD diffraction patterns of (a) Fe(0)@FeS as well as CNF-Fe(0)@FeS; (b) PKSAC-AgNPs; and (c) PTMAC [84,92,126].

peculiar to silver nanoparticles, hence establishing the crystalline nature of the carbon-based nanocomposite [84].

The EDX analysis helps in the proper identification of the elements that are present in the sample. The peak observed in the EDX image at 21° was very intense (Fig. 5a). It was observed that some new peaks were formed and some disappeared when the acid-modified mango pod was compared with the raw mango pod, hence enhancing the adsorption process [71]. The EDX image also revealed the elements that are present in a carbon-based nanocomposite. The EDX analysis is of PTMAC after methylene dye adsorption revealed well-defined peaks, which implied that the methylene blue dye bounded well onto the surface of PTMAC (Fig. 5c). However, the EDX analysis of the STMAC revealed small peaks of methylene blue dye (Fig. 5b) [126].

3.3. Scanning electron microscopy (SEM) and transmission electron microscopy (TEM)

An important characterization technique that reveals the morphology of the material is scanning electron microscopy (SEM) [127, 128]. It uses a focused beam of light to analyze and produce high magnification, complex and clear images of the composition, and also, the topography of the sample's surface [66,129]. SEM operates on the concept of using kinetic energy to generate signals from electron interactions. Furthermore, the presence or absence of well-defined pores and the pore size of the sample are well-established by SEM analysis as seen in Figs. 6 and 7. Transmission electron microscopy (TEM) is also used to understand the morphology in terms of the shape and size of the nanomaterials as displayed in Fig. 8 and 9. SEM and TEM both create images, but TEM creates its own by using electrons passing through the

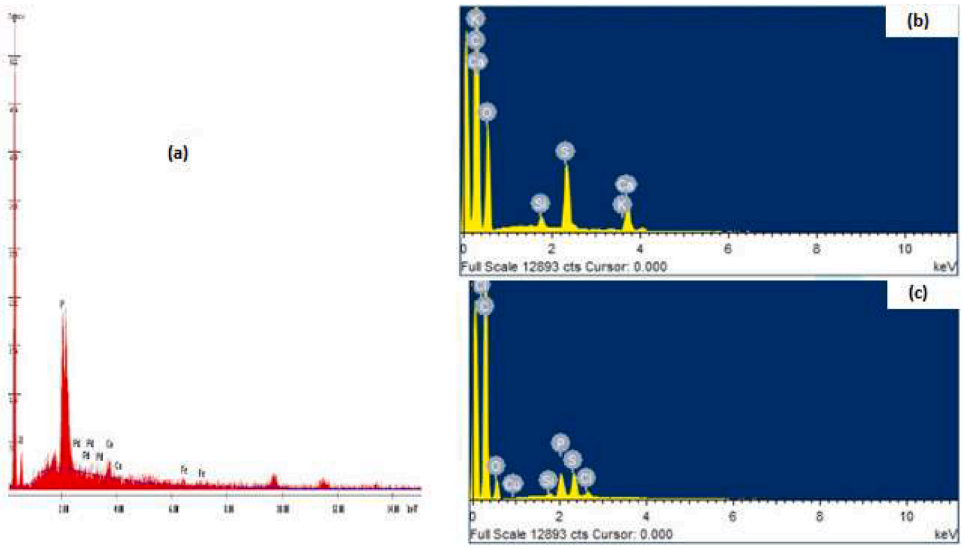

Fig. 5. (a-c): EDX elemental constituents (a) Acid-modified mango pod; (b) STMAC and (c) PTMAC [71,126].

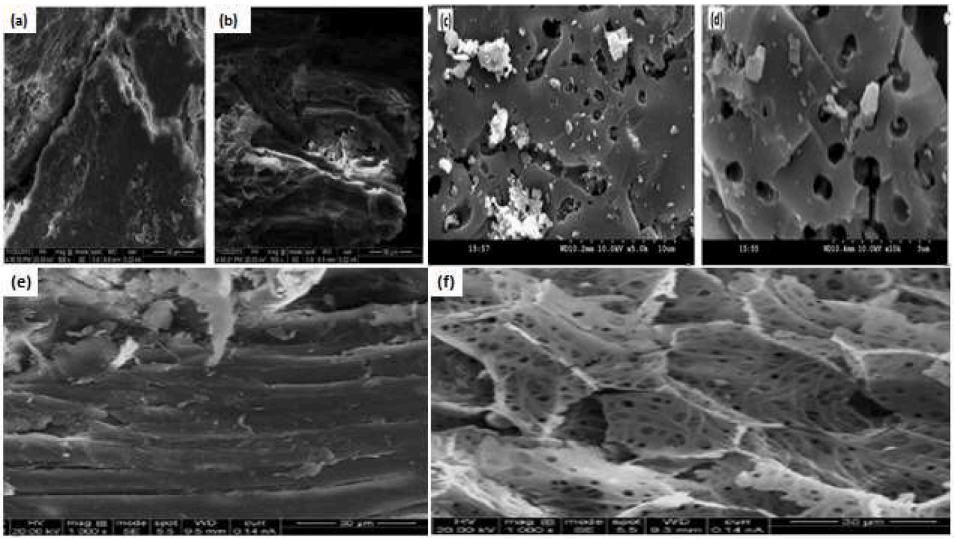

Fig. 6. (a-f): SEM surface morphology of MOSPR; Moringa seed pod activated carbon (MOSPAC); Palm kernel shell activated carbon; Raw mango pod and Acid-modified mango pod [71,84,120].

sample. SEM on the other hand uses electrons from the sample which are either reflected or even knock-off to produce an image of the sample's surface [130,131].

3.3.1. *SEM characterization*

The SEM image of the raw mango pod (Fig. 6a) was closed and characterized by a porous structure that is very poor. However, when the mango pod passed through the chemical activation process, the result of the SEM analysis carried out on it showed excellently developed pores with very good porous structure (Fig. 6b) [74]. The SEM images in Fig. (6c& 6d) reveals the morphology of the carbon-based nano-composite (PKSAC-AgNPs). The presence of pores in the cracks affirms that the carbon-based nanocomposite could be efficient for environmental clean-up processes such as adsorption [44].

Similar to this, Fig. 7(a-f) showed the morphology of bare ZnO prior to the addition of CSAC (coconut shell activated carbon) to the as-synthesised ZnO matrix to create CSAC-ZnO@600, as shown by [108]. At different magnifications, Figs. 7(a-c) and 7(d-f) show the spherical morphology of ZnO, whereas Fig. 7(d-f) shows the combination of spherical and rod-like morphology of CSAC-ZnO, which is corroborated by the TEM images. Generally, it was observed that morphological modification can be actualized by introducing an environmentally benign agro-residue source carbon as base material such as observed in CSAC–ZnO.

3.3.2. *TEM characterization*

TEM generates visuals that allow you to see even the tiniest surface or nanoparticle features. The TEM pictures from earlier research are displayed in Figs. 8 and 9. Fig. 8a exhibits a characteristic spherical nanopore of ZnO nanoparticles. The enhanced rod-like shape of the as-synthesised carbon-based CSAC-ZnO is shown in Fig. 8(b-c). The carbon-based CSAC-ZnO heterostructure's inter-spatial lattice spacing was shown in Fig. 8(d–F).

As shown by the experiments by Dada et al., 2023 in Fig. 9(a-c), information on electron mapping may be gained from the high resolution TEM. The presence of the component elements—carbon, zinc, and oxygen—as well as their distinctive colours were verified by the High Angle Annular Dark Field (HAADF) imaging. Furthermore, the carbon-

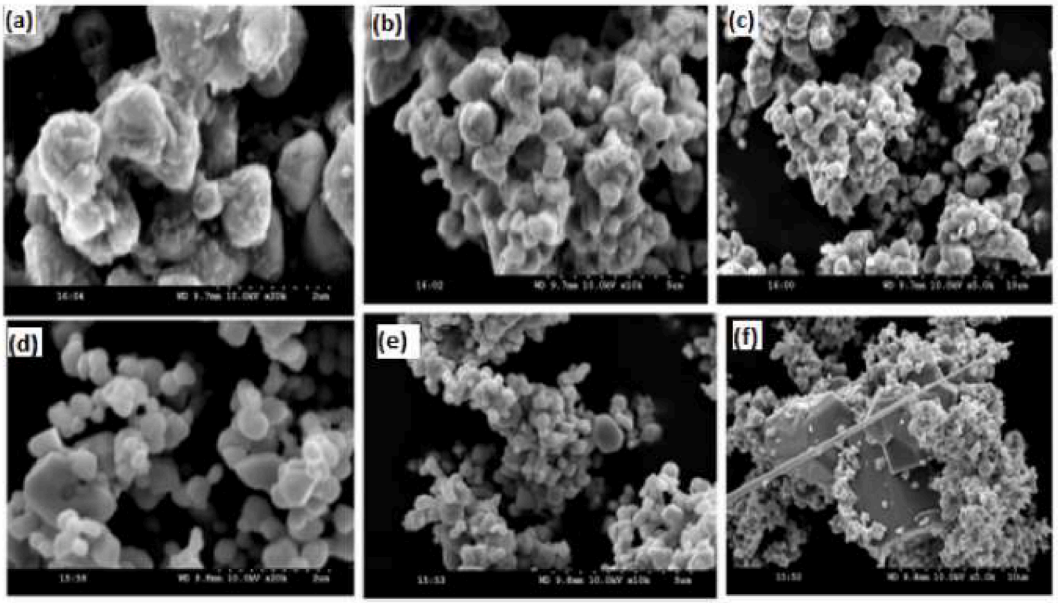

Fig. 7. (a-f): The SEM pictures of ZnO@600 °C at (a) 2 μm (b) 5 μm (c) 10 μm and SEM pictures of CSAC-ZnO@600 at (a) 2 μm (b) 5 μm (c) 10 μm [108].

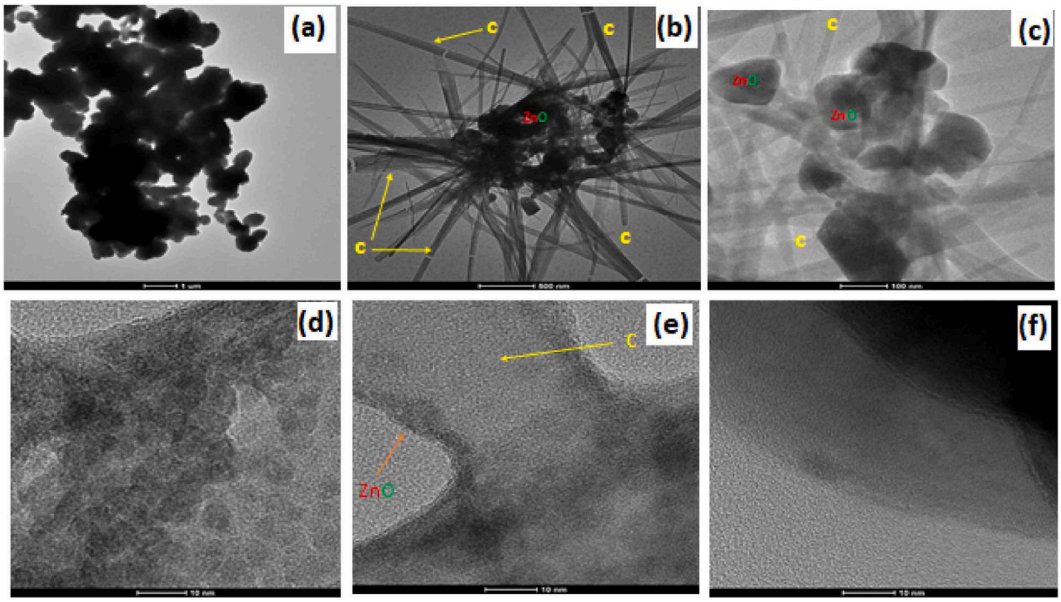

Fig. 8. (a–f): TEM morphological image (a) ZnO pure (b) TEM image of CSAC doped-ZnO (c) High resolution TEM image of CSAC-doped-ZnO; and (d, e, & f) SEAD pattern of ZnO and CSAC-ZnO [108].

based nanocomposite shown in Fig. 9(d-h) has a crystallinity that is confirmed by the Selected Area Electron Diffraction (SAED) pattern from the HR-TEM. The lattice spacing of 0.316 and 0.386 nm, which correspond to the (111) and (110) planes of pyrite FeS2, respectively, is clearly visible in Figs. 9(g-h) [108]. The TEM pictures in Fig. 8(g–h) demonstrated the sample BiOBr's nanoscale structure. The clear grain deposition on the activated carbon was visible in the picture. It confirmed that the material was highly crystalline (BiOBr). (002), (110), and (211) were the corresponding values for the spacing of 0.40 nm, 0.27 nm, and 0.40 nm, respectively [132].

3.4. The X-ray photoelectron spectroscopy (XPS)

An effective method for determining the surface properties of carbon-based materials and their nanocomposites is X-ray photoelectron spectroscopy (XPS). It makes use of the photoelectric effects concept, in which an X-ray photon is used to bombard a surface. Because it uses an ultra-high vacuum, the sample that will be probed must first be evacuated before analysis can begin. Benefitably, XPS could analyse particles as tiny as 1–10 nm. The elemental components, electrical state, binding energies, and thickness of the materials may all be usefully determined via XPS. Many factors, including formal oxidation status, local bonding environment, and nearby atom hybridization, influence the typical binding energy of any element [108,133].

From earlier research conducted by [108], the ZnO doped with carbon (CSAC-ZnO), the XPS spectra of CSAC-ZnO are shown in Fig. 10 (a–d), where the core peaks of Zn, O, and C are present together with their hybridization of Zn 2p, O 1 s, and C 1 s. Zn 2p3/2 and Zn 2p1/2 of ZnO were found to have binding energies of 1041.25 eV and 1021.2 eV, respectively. Zn–O, –OH, and C–O bonds had binding energies of 529.7,

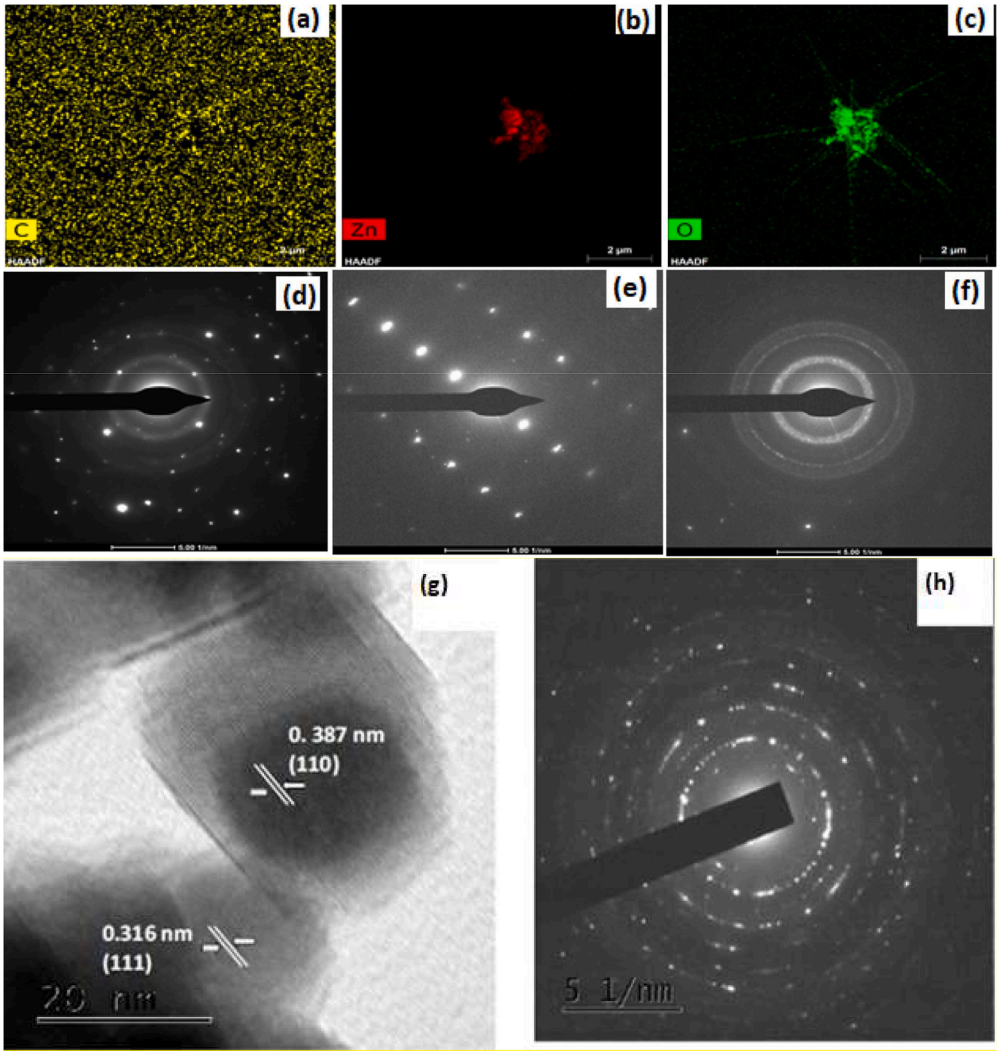

Fig. 9. (a–c): Electron mapping image of (a) HAADF for Carbon (b) HAADF for Zinc (c) HAADF for Oxygen, (d–f) SEAD pattern of CSAC-ZnO [108]; (g-h): TEM image of BiOBr composite and FeS respectively [92,132].

530.6, and 531.8 eV, whereas C–C, C–OH, and C–O bonds have binding energies of 284.5, 286.1, and 288.7 eV. This might provide more evidence in favour of the FTIR's finding that the functional groups found are present[134].

4. Cationic dyes

Dyes can be categorized based on the structures of the materials, their origin or source of the materials and the nature of the chromophore. Based on their source, dyes could be divided into natural dyes and synthetic dyes [135–138]. Natural dyes are obtained from natural sources, while synthetic dyes are derived from organic and inorganic compounds. Based on their charges, dyes can be classified into cationic dyes and anionic dyes (Fig. 11). Dyes are characterized by their deep colour and good solubility when put in a solution. They form clear solutions and can be applied to materials to give fastness [34]. Several industries (such as cosmetics, fabrics, paper, food, printing, etc.) use dyes to give colour to their products. Textile industries are found in most countries, and 93 % of their used water comes out as coloured wastewater. This is due to the presence of high concentrations of organic dye compounds and some heavy metals [1,8,139].

Cationic dyes are organic dye compounds that have polluted our environment significantly over the years [140–143]. These dyes could be separated into positively charged ions and negatively charged ions in an aqueous solution. They can work together with the negative group found on the fibre molecules to form a salt. In the process of forming the salt, they become firmly attached to the fibre, hence the fibre becomes dyed. Cationic dyes are coloured cation-releasing dyes in solution [144]. Identified as different types of cationic dyes are heterocyclic compounds, triarylmethane, anthraquinone, and azo. Examples of triarylmethane dyes are Malachite Green, Rosaniline, Fuchsin, Methyl violet, and Phenolphthalein. Pigment Yellow 108, pigment blue 60, pigment Red 177, anthrapyrimidine yellow, Indanthrone blue, and anthraquinone red respectively and are examples of anthraquinone dyes [143]. Some of the cationic dyes which have been extensively used in adsorption studies are Malachite green [37,145], Rhodamine B [32,120,146,147], Crystal violet [55,148,149] and Methylene blue [27,52,83]. Others are; Basic brown 1, Basic Violet 10, Basic Violet 10, Basic Violet 14, Basic Blue 9, Basic Blue 54, Basic Violet 3, and Basic Green 4 [138]. Cationic dyes are basic dyes that originate from a class of synthetic dyes. They are characterized by shades of colours that are bright when they are used on textile materials and some of their chemical structures are shown in Fig. 12. Cationic dyes are also very soluble in water and hence are problematic to the environment. They have a high affinity when used for wool, silk, and acrylic materials. They are not easily removed by the usual primary treatments [138]. Table 3 shows a list of some cationic dyes, the agricultural wastes they are used with and their removal efficiencies. In a past study, nanocomposites were studied for the

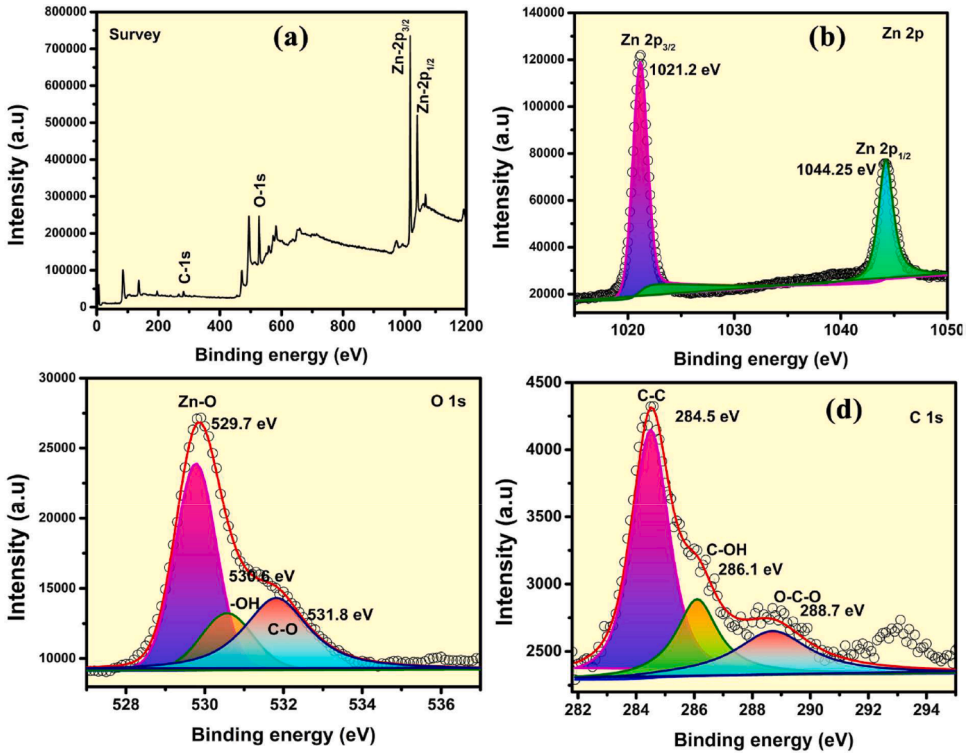

Fig. 10. (a–d): XPS spectra of CASC-ZnO@600: (a) survey spectrum; (b)–(d) high-resolution spectra of the respective Zn 2p, O 1 s and C 1 s core levels [108].

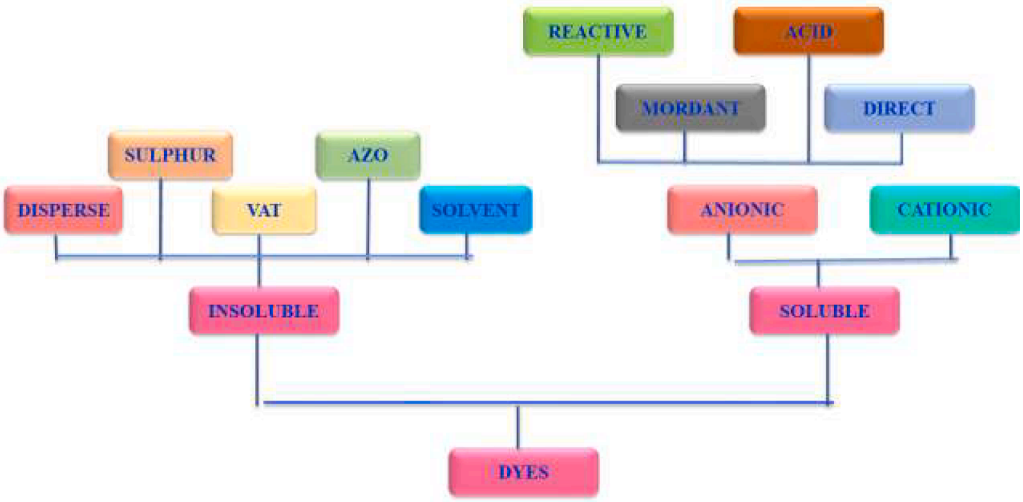

Fig. 11. Various dyes categories and classifications.

photodegradation of a cationic dye under a visible light source. The composites ZnO/algae and Co– ZnO/algae were used to degrade malachite green dye. The study further revealed that after 10 min, the nanocomposites fully degraded 5 mg/L of the malachite green at a pH of 7 [150]. In this section, cationic dyes were widely discussed.

5. Methods of dyes removal and operational techniques for adsorption of cationic dyes

The sequestration of cationic dyes from wastewater remains an interesting area of research. This has led to the suggestion and application of several removal techniques, which are presented in this section. Dyes removal has been categorized into chemical, biological and physical methods. Presented in Table 2 are various types of methods of dye removal, advantages and disadvantages as examined by researchers.

Research has shown that some of the conventional methods for treating dyes-laden effluents have not been satisfactory, in the area of removal capacity of the methods employed [8,138,143]. Treatment processes such as oxidation, ozone treatment, photo-degradation, adsorption, etc. have been employed. Amongst these techniques, adsorption is mostly preferred based on its advantages such as; its ease of operation, cost-effectiveness, and adaptation to a wide range of environmental pollutants among others. Adsorption refers to the process in which a solid material holds in molecules of a liquid or gas form a thin layer on the solid. It is usually based on a given surface (a solid) which accommodates the development of a film of the adsorbate (may be liquid or gas). Adsorption is referred to as a surface-based process while absorption emphasizes more on the volume of the material. Several

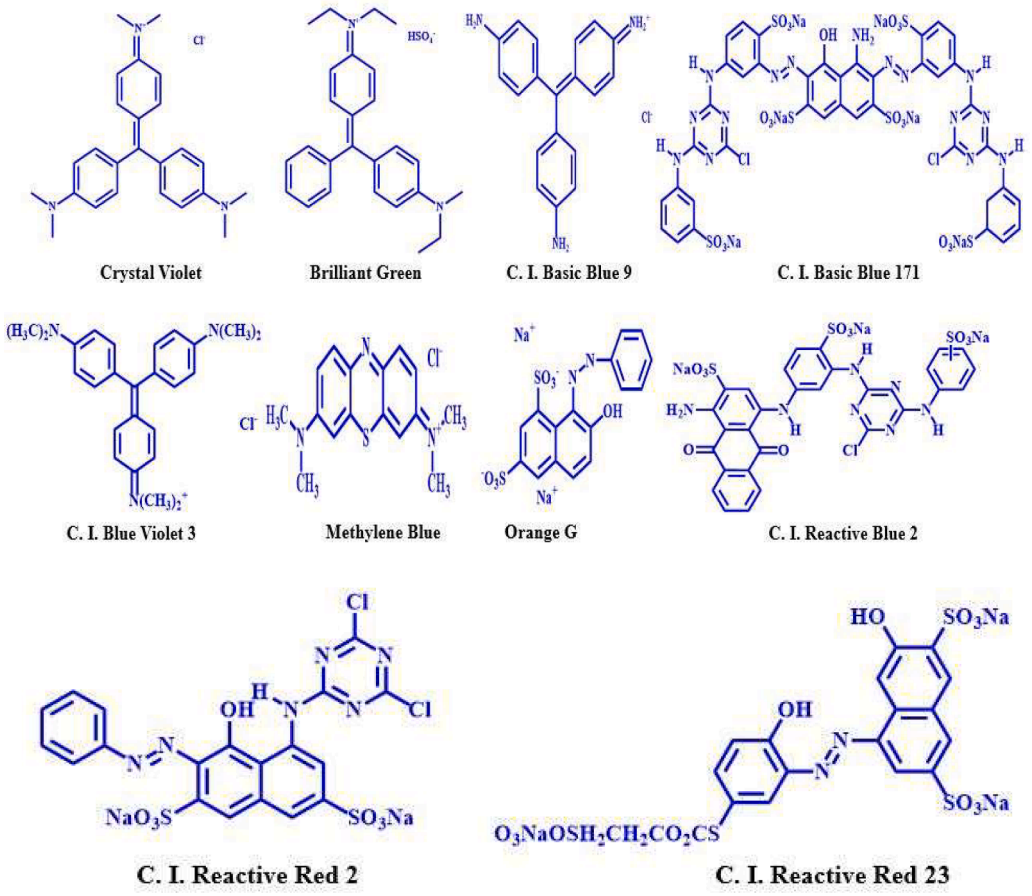

Fig. 12. Structural representation of selected cationic dyes.

researchers have investigated the efficacy of adsorption in the elimination of certain endocrine disrupting chemicals (EDCs). Different parameters are important when adsorption processes are to take place. Imperative operational techniques like initial concentration, pH, ionic strength, co-existing ions, contact time, adsorbent dose, stirring speed, etc. are all important parameters to be considered when investigating the adsorption of cationic dyes [161–163].

The procedures, importance as well as some general findings have been listed below in Table 3. Most often, the temperature is usually varied when carrying out an adsorption study [66,164]. Studying this parameter helps us to determine if a reaction is endothermic or exothermic. The pH explains the acidity or basicity of the reaction. In adsorption studies, HCl and NaOH are used to either increase acidity or reduce the acidity of a solution. The temperature has a lot to do with the success of an adsorption process.

The adsorption of a dye known as methylene blue using modified activated carbon at different pH levels was done by Kuang and his colleagues in 2020 [165]. They reported that adsorption capacities were favourable when the pH was in the alkaline range as well as when it was in its natural range. They reported that the increase in pH resulted in a simultaneous increase in the adsorption removal rate and capacities of the adsorbent. Their report included the fact that when the pH value is high, the hydroxyl groups (O—H) and carbonyl groups (C = O) which are on the adsorbent can attract the cationic dye molecules (methylene blue). According to their report, 100 mL of three different methylene blue concentrations (10, 30, and 50 mg/L) was prepared under different adsorbent doses (ranging from 5 to 100 mg) to determine the effect of the adsorbent dose. The study exhibited a rise in the uptake rate of methylene blue, as the mass of the adsorbent increased. However, at high adsorbent doses, there was a decline in the adsorption rate. This was reported to be based on the presence of insufficient molecules of dye in the solution. As the effect of initial concentration was also determined, the result of the study showed a decrease in the rate of decolourization (from 96.6% to 58.7%) and an increase in adsorption capacity (from 64.4 to 195.8 mg/g). The effect of contact time was also checked in the same study, which involved the removal of methylene blue. The researchers reported an increase in the removal rate and adsorption capacity of methylene blue when contact time was increased. They reported that when the initial concentration of the dye is lowered, a lesser time is needed to achieve equilibrium [165]. Since, we are concentrating more on the cationic dyes, the contact time of an adsorption process basically refers to the amount of time an adsorbent use in contact with the dye solution. The removal rate can either decrease or increase based on the contact time between the adsorbent and the adsorbate. The effect of initial dye concentration in an adsorption process can be well studied when the adsorbent dosage remains constant. Initial concentration can be varied from 10 to 50 mg/g. The rate of adsorption can be faster at high concentrations before it attains equilibrium. How porous the activated carbon sample is, goes a long way in determining the level of adsorptive affinity of the adsorbent in an adsorption process [166].

The effect of adsorbent dose on adsorption capacity was explained in 2019 by some researchers who looked into the adsorption of phenol. Their adsorbent was silver-gold nanoparticle-assisted mango seed. They reported an increase of 58.6% and 72.4% in the capacity of adsorption when the adsorbent dose was increased from 0.1 - 0.5 g. This could be due to an increase in the adsorption site. From previous studies carried out by various researchers, list of cationic dyes, their operational conditions for maximum adsorption at optimum conditions as well as the removal efficiency are listed in Table 4. From Table 4, least percentage

Table 3
Relevant operational parameters and brief descriptions.

Operational Parameters	Established procedure & Principle of the Procedure	Importance	General findings	References
Effect of Initial concentration	First, the amount of solute to be used would be weighed and set aside. This should be followed by the determination of the number of grams present in a mole of the solute. Also, the solvent to be used should be measured. Concentrations could be varied between 10 and 50 mg/L. Calculations should be done using this formula.	It directs the operational pathways. It serves as a main driving force to overthrow all mass transfer resistance of the cationic dyes. It determines the uptake of the adsorbate by the adsorbent.	Initial concentration was used for the photodegradation studies by Wu& Zhang in 2004. The Rhodamine blue solution changed to a colourless solution, showing that an effective photodegradation had occurred. When concentration is low, adsorption is always higher.	[151]
Effect of contact time	Plotting adsorption percentage against adsorption time	The data gotten from the adsorption process at specific time (t) help in the study of adsorption dynamics	The equilibrium time is dependent on the concentration	[5,57,152]
Effect of temperature	The temperature will be varied with percentage adsorption.	It aids both desorption and adsorption studies.	As temperature increases, adsorption rate decreases.	[5,153]
Effect of pH	1 g of each sample will be weighed and put in beakers. These samples will then be boiled for 5 mins. After which, it will be allowed to cool down, so the temperature can reduce to room temperature. Then the pH will be taken.	Useful in determining effect of temperature, contact time and adsorption rate.	As pH increases, adsorption rate may be higher or lower.	[16,147, 154,155]
Effect of ionic Strength	This could be done with the use of NaCl solution of different which have different ionic strengths. This can range from 0.001 M to 1.0 M.	It helps in determining the measure of the concentration of ions in that solution.	The ionic strength has been discovered to increase as the current increases. Also, efficiency is proportional to electrolyte ionic strength.	[156,157]
Effect of co-existing ions	This is carried out within a binary solution containing the adsorbate and one cation or anion at a chosen pH.	To know if there is an increase or decrease in adsorption capacity.	It shows the impact of cations and anions on the adsorption of the adsorbate.	[158]
Effect of adsorbent dose	Different doses will be prepared and will be utilized during the adsorption process.	The increase in adsorbent dose often leads to an increase in adsorption percentage.	Sometimes, a competition between the adsorbate could result to a decrease in adsorption percentage even if the adsorbent dose is increased.	[147,159, 160]
Effect of stirring speed	Different agitation or stirring speeds will be worked with. It could be between 120 rpm and 240 rpm. Removal efficiencies will be observed	Useful in determining optimum agitation speed	Significant changes may either occur or not during this process.	[143]

removal efficiency of 75% was observed in Malachite green adsorption onto Functionalized maize cob (FZMC) [167] while 100% removal efficiency was observed for adsorption of methylene blue onto waste black tea powder [5].

6. Adsorption isotherm, kinetics and thermodynamics modelling in brief

Specifically, the adsorption isotherm, kinetics, and thermodynamics modelling are the focal points of this section.

6.1. Isotherm modelling

The interactions that take place between the adsorbents and the adsorbate can be better understood by using isotherm models. Langmuir, Freundlich, Temkin, and Dubinin-Kaganer-Raduskevich (DKR) are the four main two-parameter isotherm models that are often used to describe equilibrium data. Table 5 shows the list of various adsorbents used for cationic dyes adsorption as well as best isotherm that well described the equilibrium data in a batch adsorption studies. Ranking of the monolayer adsorption capacity (Qmax) of those adsorbents were also explored. The previous section described the nitty-gritty of most commonly applied four isotherm models. Non-linear models are frequently more precise in representing adsorption data, particularly when the adsorption does not completely adhere to the assumptions of adsorption models. Non-linear models are suitable for analyzing real experimental data and are frequently employed in situations where a high level of accuracy is necessary. Linear models may incorporate inaccuracies as a result of the translation process, but they simplify the mathematical calculation of the different adsorption parameters and foster quick approximations. The non-linear equations and the linear equations of the isotherms and kinetic models are further described below [174,175].

6.1.1. Langmuir isotherm model

The Langmuir model gives a general assumption that one gas molecule is adsorbed in each of the adsorption sites. This is a monolayer adsorption model with the uptake of dyes and other contaminants at finite, specific, and identical localized sites with no interaction between adsorbed molecules and adjacent sites. Another remarkable fact about Langmuir is that it has been seen to fit most studies much more than other employed models. A study in 2018 revealed that data from the equilibrium adsorption were in line with the Langmuir model. The value of R^2 was 0.988 which is close to 1. The researchers adsorbed malachite green dye making use of palm kernel shells as the adsorbent. The study confirmed that the Langmuir isotherm fitted the adsorption process better [101]. In 2016, a study by Dada et al. confirmed that Langmuir isotherm best described the experimental data obtained from the use of a nanocomposite derived from bamboo and manganese, which was called bamboo-supported manganese (BS-Mn). A cost-effective approach was used to manufacture a nanoparticle, iron-doped ZnO nanoparticles (Fe–ZnO) using shrimp-shell. Langmuir isotherm was reported to best describe the data generated with a maximum monolayer capacity of 83.81 m/g [105]. The non-linear and linear models of Langmuir isotherm equation are presented in Eqs. (1) and (2).

$$q_e = \frac{q_m K_L C_e}{1 + K_L C_e} \tag{1}$$

Langmuir's isotherm is generally represented by this linear equation;

$$\frac{C_e}{Q_e} = \frac{1}{Q_{max} K_L} + \frac{C_e}{Q_{max}} \tag{2}$$

$$R_L = \frac{1}{1 + K_L C_0} \tag{3}$$

Table 4
List of some cationic dyes and their operational conditions for maximum removal efficiencies.

Cationic dyes	Adsorbents used	Equilibrium conditions at optimum.	Removal efficiency	References
Rhodamine B	*Moringa oleifera* seed pod	pH = 3.01, contact time = 120 mins, initial conc. = 1000 mg/L, Temp = 303 K, adsorption uptake = 1014.99 mg/g Adsorbent dose= 96.43 mg/g	94.76%	[32]
Malachite green	Zea Mays Cob (FZMC)	pH = 8, contact time = 120 mins, initial conc. = 500 ppm, Temp = 298 K, Q_{max} of FZMC = 64.52 mg/g	75.11%	[167]
Rhodamine B and Malachite green	Modified *Irvingia gabonensis* nut waste (MIg)	pH = 6, contact time = 120 min, initial conc. = 500 ppm, Temp = 26 °C, Adsorbent dose = 250 mg/g	99.90%	[168]]
Methylene blue	Waste black tea powder	pH = 3 – 11, contact time = 60 mins, initial conc. = 1000 mg/L, Temp = 26 °C, Adsorbent dose = 302.63 mg/g	100%	[151]
Methylene blue	Coconut coir dust	pH = 6, contact time = 20 min, initial conc. = 50 mg/L, shaking speed = 200 rpm, Temp = 27 °C, Adsorbent dose = 0.1 g	99.50%	[169]
Methylene Blue	Cucumis sativus peel (CSP) waste	pH = 8, contact time = 120 min, initial conc. = 100 mg/L, Temp = 298 K, Adsorbent dose = 4 g/L	81.40%	[170]
Malachite green	*Luffa aegyptica peel (LAP)*	pH = 7, contact time = 150 min, initial conc. = 25–100 mg/L, Temp = 303 K, Adsorbent dose = 0.6 g/L	89.20%	[171]
Methylene blue	Corn cob sources waste from plant	pH = 6.1, contact time = 24 hrs, initial conc. = 50 mg/L, Temp = 308 K, Adsorbent dose = 0.5 g/L	97%	[172]
Malachite green	Durian seed	pH = 8, contact time = 120 min, initial conc. = 100 mg/L, Temp = 298 K, Adsorbent dose = 0.25 g/L	97%	[173]
Malachite green	Palm kernel shells	pH = 6, contact time = 40 min, Temp = 328 K, Adsorbent dose = 0.5 g/L	–	[148]

Where;

Q_e= The quantity of adsorbate that is adsorbed per unit weight of adsorbent at equilibrium (mg/g)

C_e = This is the concentration of adsorbate at equilibrium in solution after adsorption (mg/L)

Q_{max} = Maximum adsorption capacity (mg/g)

K_L = Langmuir adsorption equilibrium constant (L/mg)

$R_{L=}$ dimensionless separation factor

C_0 = Initial adsorbate concentration

R_L gives an insight into the nature of adsorption and whether an adsorption process was favourable or not favourable. Significantly, the separation parameters specifically situate the adsorption process to be favourable when R_L is greater than zero but less than unity ($0<R_L<1$), unfavourable when R_L is greater than unity ($R_L>1$), adsorption is linear when R_L is equal to unity ($R_L=1$) and irreversible adsorption occurs when R_L is equal to zero [167,176]. In a study on the adsorption of malachite green onto the peel gotten from Luffa aegyptica, the R_L fell between 0 and 1 denoting that the adsorption process was favourable at a temperature of 303 K and initial concentrations ranging from 25 to 100 mg/g [171]. Also, the values obtained for R_L in the study using functionalized mango for rhodamine B dye removal were between 0 and 1, which also denoted the favourable adsorption process (scavenging).

6.1.2. *Freundlich isotherm*

Freundlich model helps to estimate the adsorption concentration of the adsorbent when it absorbs the adsorbate used. Some of its assumptions are; surface roughness, heterogeneity, and adsorbate-adsorbate interactions. This model sometimes doesn't fit some studies. Generally, this isotherm helps in describing the adsorption characteristics of a heterogeneous surface. In 2014, a group of researchers used durian seed to chemically prepare activated carbon to adsorb Malachite green (MG) dye. The experimental data were analysed using eight different kinetic models. However, the Freundlich isotherm was discovered to be the best fit for the experimental data. With the R^2 of 0.9995, it showed the favourability of the adsorption process [173]. In 2019, a study was carried out and the outcome showed that adsorption isotherms for methylene blue and phenol were the best fit for the Freundlich model. The R^2 was 0.881 and 0.978 respectively [27].

$$\text{Freundlich isotherm is non} - \text{linearly represented by}: \; q_e = K_F C_e^{1/n_F} \tag{4}$$

It is linearly expressed as Eq. (5):

$$\log q_e = \log k_F + \frac{1}{n_F} \log C_e \tag{5}$$

q_e =the quantity adsorbed at equilibrium

C_e = Equilibrium concentration of adsorbate (mg/L)

k_f = Freundlich constant representing adsorption capacity

n_F= Adsorption intensity

The $\frac{1}{n_F}$ is a parameter in the Freundlich equation that shows the heterogeneity of the adsorbent's surface. Heterogeneity increases with a decrease in the value of 1/n. When the value of $\frac{1}{n_F}$ is below unity, then it shows a normal adsorption process. The adsorption process has been well described utilizing the Freundlich adsorption intensity (1/n) which is also used to determine the strength of the adsorption process. Adsorption is said to be normal and favourable when the value of 1/n is below unity. Cooperative adsorption is obtained when the value of 1/n is above unity. However, n being equal to unity is an indication of independence of the partition between the two phases of concentration [33, 170].

6.1.3. *Temkin isotherm model*

In this model, the behaviour of the interaction between the adsorbent and the adsorbate is emphasized. This model proposes that the heat of adsorption of all molecules in the layer decreases linearly with the

Table 5
Best fitted isotherm, kinetic, thermodynamics modelling with maximum monolayer adsorption capacities of different agro-residue.

S/N	Adsorbent used	Isotherm model best fitted	Q_{max} (mg/g)	Kinetics model best fitted	Thermodynamics Parameters	References
1	Raphia hookerie fruit epicarp	Freundlich	666.67	Pseudo Second order	$\Delta G^\circ = -3.122$ kJ/mol, $\Delta H^\circ = 11.74$ kJ/mol, $\Delta S^\circ = 49.23$	[98]
2	Functionalized thuja cone carbon (FTCC)	Freundlich	83.4	Pseudo Second order	$\Delta G^\circ = -15.67$ kJ/mol, $\Delta H^\circ = 49.48$ kJ/mol, $\Delta S^\circ = -0.11$	[146]
3	Palm kernel	Langmuir	225	Pseudo Second order	ΔG° was negative	[101]
4	bamboo-supported manganese (BS-Mn) nanocomposite	Langmuir	44.64	Pseudo Second order	$\Delta G^\circ = -31.73$ kJ/mol, $\Delta H^\circ = 202$ kJ/mol, $\Delta S^\circ = 107.2$	[120]
5	Bamboo (*Bambusa vulgaris*)	Freundlich	558.29	–	–	[103]
6	Fe/ZnO-shrimp shell nanocomposite	Langmuir	83.81	Pseudo Second order	$\Delta G^\circ = -71.60$ kJ/mol, $\Delta H^\circ = 29.02$ kJ/mol, $\Delta S^\circ = 0.142$	[62]
7	Corn cob powder	Langmuir	46.28	Pseudo Second order	$\Delta G^\circ = -7.6$ kJ/mol, $\Delta H^\circ = 37.44$ kJ/mol, $\Delta S^\circ = 158.783$	[122]
8	Novel biosynthesized silver nanoparticles (AgNPs)	Langmuir	59.85	Pseudo Second order	$\Delta G^\circ = -6.13$ kJ/mol, $\Delta H^\circ = 62.11$ kJ/mol, $\Delta S^\circ = -184.01$	[133]
9	Rice Husk Biochar-Based Magnetic Nanocomposite	Langmuir	185.6	Pseudo Second order	–	[53]
10	*Moringa Oliveira* seed pod activated carbon (MOSPAC)	Langmuir	1250	Pseudo Second order	$\Delta G^\circ = -27.381$ kJ/mol, $\Delta H^\circ = 127.562$ kJ/mol, $\Delta S^\circ = 507.894$	[73]
11	*Ocimum gratissimum* leave (OGL)	Freundlich	77.52	Pseudo Second order	$\Delta G^\circ = -5.759$ kJ/mol, $\Delta H^\circ = 1.178$ kJ/mol, $\Delta S^\circ = -127.786$	[147]
12	durian seed-based activated carbon	Freundlich	445.6–532.3	Pseudo Second order	$\Delta G^\circ = 11.43$ kJ/mol, $\Delta H^\circ = 10.64$ kJ/mol, $\Delta S^\circ = 12.56$	[138]
13	Coconut coir dust	Freundlich	29.50	Pseudo Second order	$\Delta G^\circ = ?7.80$ kJ/mol, $\Delta H^\circ = 37.56$ kJ/mol, $\Delta S^\circ = 112.2$	[134]
14	Coconut Shell-Based Activated Carbon	Langmuir	214.63	Pseudo Second order	$\Delta G^\circ = -30.91$ kJ/mol, $\Delta H^\circ = 25.69$ kJ/mol, $\Delta S^\circ = 111.88$	[48]

surface coverage [146,177,178]. The non-linear and linear eqautions of Temkin model is expressed in Eqs. (6) and (7).

$$\text{The non} - \text{linear equation is given as}: \quad q_e = \frac{RT}{b_T} \ln (K_T C_e) \tag{6}$$

The linear equation of the Temkin model is given as;

$$q_e = \frac{RT}{b_T} \ln A_T + \frac{RT}{b_T} \ln C_e \tag{7}$$

Where;

b_T = Temkin constant (It is related to the adsorption temperature). Its unit is J/mol

R = Gas constant (which is 8.314 J/mol)

T = Absolute temperature in Kelvin

B = Temkin constant

K_T = Temkin isotherm equilibrium binding constant. It is measured in L/g

6.1.4. *Dubinin-Radushkevich (D-R) adsorption isotherm*

The D-R equation for micro-porous solids was founded by Dubinin and his colleagues.D-R isotherm helps to determine the adsorption mechanism, unlike Langmuir and Freundlich who do not suggest adsorption mechanisms. The isotherm can be used for micro-porous solids which are characterized by uniform microporous structures. A major use of this isotherm is that it helps to distinguish between chemical adsorption (i.e., chemisorption) and physical adsorption (i.e., physisorption) [179,180]. Given in Eq. (8) is the D-Rmodel:

The non-linear model is expressed as:

$$q_e = q_m \exp^{(-k\varepsilon^2)} \tag{8}$$

The linear equation is expressed as expressed in Eq. (9):

$$lnQ_e = lnQ_m - A_{D-R}\varepsilon^2 \tag{9}$$

Where:

Q_e = The amount of adsorbate at equilibrium

Q_m = Theoretical isotherm saturation capacity (mg /g)

A_{D-R} = isotherm constant related to sorption energy (mol^2kJ^2)

ε = Polanyi potential (kJ^2mol^{-2})

However, ε can be derived from the following

$$\varepsilon = RTln\left(1 + \frac{1}{C_e}\right) \tag{10}$$

Where:

Other parameters are as previously defined. Experimental parameters are generated from the plot of lnQ_e against ε^2. Research has demonstrated that the energy of adsorption might be assessed utilizing E = -[$1/\sqrt{2A_{D\text{-}R}}$] and this may be used to classify the adsorption mechanism as either physisorption if E < 8 $kJmol^{-1}$ and chemisorption if E > 8 $kJmol^{-1}$ [167,154].

In Table 5, the best fitted isotherm model for each carbon-based nanocomposite and a variety of Q_{max} values for activated carbon derived from agro-waste are comparatived. The Langmuir and Freundlich models were found to be the most effective in illustrating the properties of the materials utilized, out of all the isotherm models that were mostly fitted to the equilibrium data.

6.2. *Adsorption kinetics, mechanisms of cationic dyes*

The kinetics and mechanistic study of the adsorption process are very important because the information obtained helps determine the rate and the ruling mechanism. The parameters evaluated could also be applied in thermodynamics studies. Listed in Table 5 are the list of selected adsorbent previous used for adsorption of cationic dyes with pseudo-second order being the best kinetic model that best analysed the kinetics data.

6.2.1. *Pseudo-First kinetics model*

Generally, pseudo-first order expression is applied in the adsorption kinetic study to investigate the rapid rate of interaction in a solid-liquid-based system. Although, most adsorption processes are not always best described by this model based on low regression coefficient (R^2) values. The non-linear and linear equations of Pseudo-first order adsorption kinetics are presented in Eqs. 11 and (12).

Its non-linear equation is given as:

$$q_t = q_e\left(1 - e^{-k_1 t}\right) \tag{11}$$

Its linear equation is given in Eq. (12) as:

$$\log(q_e - q_t) = \log q_e - \frac{k_1 t}{2.303} \tag{12}$$

Where q_e refers to the quantity of the substance that is adsorbed at equilibrium per unit weight of the adsorbent. It is measured in mg/g. q_t refers to the quantity of pollutant adsorbed at any chosen time (mg/g) and k_1 is the pseudo-first-order rate constant. Its unit is min^{-1}. The model of the pseudo-first-order is always better compatible with weak concentrations of the aqueous solution. Most of the time, this model does not fit the most adsorption kinetics studies.

6.2.2. Pseudo-Second order kinetics model

$$\text{Its non} - \text{linear equation is given as}: \; q_t = \frac{q_e^2 k_2 t}{1 + q_e k_2 t} \tag{13}$$

The linear equation of pseudo-second–order is generally expressed in Eq. (14);

$$\frac{t}{q_t} = \frac{1}{k_2 q_e^2} + \frac{t}{q_e} \tag{14}$$

When t moves towards 0, h_2 is defined as:

$$h_2 = k_2 q_e^2 \tag{15}$$

$$\frac{t}{q_t} = \frac{1}{h_2} + \frac{t}{q_e} \tag{16}$$

Where;

h_2 = initial adsorption rate for pseudo-second-order. The plot for the pseudo-second-order will be t/q_t against t. Most data of adsorption kinetics are best described by a pseudo-second-order model with R^2 very close to unity [177,178].

6.2.3. Elovich model

This model is used largely for systems in which the exterior part or surface of the adsorbent is heterogeneous in nature. The Elovich model describes how gas molecules are adsorbed into the adsorbent's surface [171]. The Elovich model explains the chemisorption of gases and therefore, aids in chemisorption kinetics. This model is represented by these equations below:

$$\text{The non} - \text{linear equations are}; \; q_t = \frac{1}{\beta} ln(\alpha\beta) + \frac{1}{\beta} ln(t) \tag{17}$$

$$q_t = ln\left(\frac{\alpha}{\beta}\right) + \frac{1}{\beta} ln(t) \tag{18}$$

Where q_t is the amount of adsorbate that is adsorbed at any time t, α refers to the initial adsorption rate (mg/g.min), β refers to the surface coverage extent and the activation of energy for chemisorption (g/mg). The t is the contact time (min), while $\frac{1}{\beta}$ refers to the number of sites that are vacant for adsorption.

6.2.4. Intraparticle diffusion model

This model describes the external mass transfer, bulk transportation, and pore diffusion behaviour of the solute molecules [136]. The intraparticle diffusion equation is represented with this equation;

$$q_t = k_{id} t^{0.5} + C \tag{19}$$

Where; k_{id} is the intraparticle diffusion rate constant ($mg.g^{-1}min^{0.5}$)

C refers to the intercept indicating the boundary thickness

q_t is the amount of solute adsorbed per unit weight of adsorbent per time, (mg/g), and $t^{0.5}$ is the half adsorption time ($min^{0.5}$)

Top-fitting kinetics and mechanism models are shown in Table 5. It was evident that the adsorption dynamics were dominant when the majority of the adsorption rate best suited pseudo-second-order and intraparticle diffusion.

6.3. Thermodynamics modelling of cationic dyes

The thermodynamic parameters usually show the possible nature of adsorption. These parameters are; Gibbs free energy (ΔG^o), enthalpy (ΔH^o), and entropy (ΔS^o). The thermodynamics reveals whether adsorption is feasible or not. Thermodynamic functions aid in comprehending the efficiency of a dye removal process by assessing three crucial factors: spontaneity, heat transfer, and entropy. The spontaneity of a process, as determined by the Gibbs free energy, indicates whether the process occurs spontaneously and this could be determined based on the experimental behaviour of the system. A negative value of Gibb's free energy denotes the feasibility and spontaneity of the thermodynamics system while the positive value indicates non-spontaneity and a non-feasible system. The adsorption process's regulating mechanism has always been crucial for evaluating chemical reactions and estimating mass transfer [29,181]. A low number indicates that the dye is quickly and effectively removed. Heat exchange, specifically enthalpy, indicates whether a process absorbs or releases heat. This information allows us to determine if higher or lower temperatures are more effective in removing dye. Entropy is a measure of randomness, and it represents the level of disorder in a process. A higher level of disorder usually corresponds to more effective removal of dye. Through the examination of all of these factors, we can assess the efficacy of the process and identify strategies to enhance its effectiveness [71,177,181]. A study in 2020 reported that the thermodynamic parameters affirm the spontaneity, randomness and feasibility of the adsorption process [124]. The data are usually subjected to Van't Hoff's equation (Equ. 14 and 15). As long as the research is conducted at various temperatures and a consistent, ideal concentration, the Kc values could be obtained from the ratio of Qe to Ce (Qe/Ce). A linear plot of log Kc against 1/T helps in extrapolating the values of ΔH^0 and ΔS^0 . If the value of ΔG^o is negative, feasible as well as spontaneous reaction suffices and non-feasible/non-spontaneous if the value of ΔG^o is positive. Eqs. (22) or (23) could be used to determine the values of ΔG^o. The process is reported endothermic if the values of enthalpy (ΔH^0) is positive while the negative value of ΔH^0 categorized the reaction as exothermic in nature. The measure of the degree of disorderliness is ΔS^0 which is the randomness of the system. The negative and positive values will denote the increase or decrease in the randomness/disorderliness of the adsorption system. When it is negative, it means the system is less disorderly (or we say entropy has reduced), however, when the value obtained is positive, the system is said to be more disorderly (i.e., there is an increase in the degree of disorderliness or increase in entropy). As reported by Dada et al. [182], the mechanism could be determined from the parameters of activation energy (Ea) using the Arrhenius equation (Eq. 21) [30,138].

$$\log K_c = \frac{\Delta S}{2.303R} - \frac{\Delta H}{2.303RT} \tag{20}$$

$$ln\, K_c = ln\, A - \frac{Ea}{RT} \tag{21}$$

$$\Delta G = -2.303RTlog\, Kc \tag{22}$$

$$\Delta G = \Delta H - T\Delta S \tag{23}$$

The value of Kc could also be obtained from the Langmuir adsorption isotherm or pseudo-second-order rate constant for studies carried out at different temperatures. The reaction is reported to be exothermic with negative Ea and endothermic reactions with positive Ea. The mechanism is physisorption if the value of Ea lies between 5 – 20 kJ mol^{-1}, and chemisorption mechanism if the value of Ea exists in the range of 20 – 400 $kJmol^{-1}$ [28]. From Table 5, it could be inferred that 99% of studies

carried out were feasible with a negative value of Gibb's free energy.

7. Conclusion and future prospect

This review has emphasized the environmental impacts of cationic dyes and the use of carbon-based nanocomposites developed with low-cost agricultural wastes as precursors for adsorbing cationic dyes. Various techniques for the development of both activated carbon and carbon-based nanocomposites were explored. The unique properties of both the carbon precursor and carbon-decorated nanocomposites were demonstrated from the spectroscopic, morphological and crystallized characterization using FTIR, XRD, SEM, TEM, EDX and XPS. The application of the developed carbon-loaded nanocomposites in efficient adsorption of endocrine disruptive cationic dye compounds, conditions for operational parameters for effective adsorption as well as the prevailing modelling for analysing equilibrium, isotherm, kinetics, and thermodynamics data were investigated. Most equilibrium data fitted to isotherm models were best described by Langmuir and Freundlich isotherm models. Observation from previous studies demonstrated that the Freundlich isotherm model best described most cationic dye adsorption using agro-waste-based carbon while the Langmuir isotherm model best described adsorption equilibrium data when carbon-decorated nanocomposites were used for cationic dye adsorption. Kinetic data were generally best fitted to pseudo-second order model and most thermodynamics studies demonstrated feasibility, spontaneity, degree of randomness as well as the domination of the endothermic nature of the system. This review provided more insight into the effective removal of cationic dyes from wastewater using nanocomposites based on carbon derived from agricultural residues, the prevailing conditions and adsorption data analytical modelling. The review is very simplified and encompassing, such that it provides the technical know-how and knowledge required for effective agro-based activated carbon and carbon-based nanocomposite syntheses, characterization, adsorption processes and adsorption data modelling. The future prospects could focus on the in-depth as well as operation of applied carbon-based nanocomposites to anionic dyes, pharmaceutical and personal care products (PPCPs), pesticides, herbicides, Per-and polyfluoroalkyl substances (PFAS) and other endocrine disruptive compounds.

CRediT authorship contribution statement

Adewumi O. Dada: Conceptualization, Methodology, Data curation, Resources, Formal analysis, Validation, Writing – review & editing, Supervision, Project administration. **Adejumoke A. Inyinbor:** Validation, Writing – review & editing, Supervision. **Bukola T. Atunwa:** Investigation, Writing – original draft. **Spandana Gonuguntla:** Resources, Writing – review & editing. **Olugbenga S. Bello:** Resources, Writing – review & editing. **Folahan A. Adekola:** Resources, Writing – review & editing. **Ujjwal Pal:** Resources, Writing – review & editing.

Declaration of competing interest

The authors declare clearly that there is no competing financial interests or personal relationship that could have instigated to influence the work reported in this paper.

Data availability

Data will be made available on request.

Acknowledgement

The corresponding author (**Dada, Adewumi Oluwasogo**) appreciated the research exposure via Post-Doctoral Fellowship funded by The World Academy of Science – Council of Scientific and Industrial Research (TWAS-CSIR) undertaken at CSIR-Indian Institute of Chemical Technology, Hyderabad, India. The CSIR-TWAS Post-Doctoral Fellowship (FR: 3240316962)

References

[1] E. Nakkeeran, S.J. Varjani, V. Dixit, A. Kalaiselvi, Synthesis, characterization and application of zinc oxide nanocomposite for dye removal from textile industrial wastewater, Indian J. Exp. Biol. 56 (2018) 498–503.
[2] Y. Chen, J. Shi, Q. Du, H. Zhanga, Y. Cu, Antibiotic removal by agricultural waste biochars with different forms of iron oxide, RSC. Adv. 9 (2019) 14143–14153, https://doi.org/10.1039/c9ra01271k.
[3] C. Mejías, J. Martín, J.L. Santos, I. Aparicio, E. Alonso, Occurrence of pharmaceuticals and their metabolites in sewage sludge and soil: A review on their distribution and environmental risk assessment, Trends Environ. Anal. Chem. 30 (2021), https://doi.org/10.1016/j.teac.2021.e00125.
[4] T.A. Aragaw, B.A. Mekonnen, Current plastics pollution threats due to COVID-19 and its possible mitigation techniques: a waste-to-energy conversion via Pyrolysis, Environ. Syst. Res. (Heidelb) 10 (2021), https://doi.org/10.1186/s40068-020-00217-x.
[5] A.O. Dada, D.F. Latona, O.J. Ojediran, O.O. Nath, Adsorption of Cu (II) onto bamboo supported manganese (BS-Mn) nanocomposite: Effect of operational parameters, kinetic, isotherms, and thermodynamic studies, J. Appl. Sci. Environ. Manage. 20 (2016) 409–422. –422.
[6] D.P. Dutta, S. Nath, Low cost synthesis of SiO2/C nanocomposite from corn cobs and its adsorption of uranium (VI), chromium (VI) and cationic dyes from wastewater Dimple, J. Mol. Liq. 269 (2018) 140–151, https://doi.org/10.1016/j.molliq.2018.08.028.
[7] S. Amirahmadi, O. Moradi, S. Arab-Salmanabadi, The adsorption of direct red 23 as a toxic pollutant in aqueous solution by using surface modified metal-organic framework containing tricarboxylic acid benzene ligand, Desalination Water Treat 317 (2024) 100132, https://doi.org/10.1016/j.dwt.2024.100132.
[8] S. Mani, P. Chowdhary, R.N. Bharagava, Textile Wastewater dyes: Toxicity Profile and Treatment approaches, in: Emerging and Eco-Friendly Approaches For Waste Management, Springer, Singapore, 2018, pp. 219–244, https://doi.org/10.1007/978-981-10-8669-4_11.
[9] J. Khodayari, K. Zare, O. Moradi, M. Kalaee, N.Mohammad Mahmoodi, Synthesis of eco-friendly carboxymethyl cellulose /metal–organic framework biocomposite and its photocatalytic activity, J. Photochem. Photobiol. a Chem. 446 (2024) 115097. https://doi.org/10.1016/j.jphotochem.2023.115097.
[10] S. Yadav, A. Asthana, A.K. Singh, R. Chakraborty, S.S. Vidya, M.A.B.H. Susan, S.A. C. Carabineiro, Adsorption of cationic dyes, drugs and metal from aqueous solutions using a polymer composite of magnetic/β-cyclodextrin/activated charcoal/Na alginate: Isotherm, kinetics and regeneration studies, J. Hazard. Mater. 409 (2021) 124840, https://doi.org/10.1016/J.JHAZMAT.2020.124840.
[11] A. Dent, R. Selvaratnam, Measuring magnesium – Physiological, clinical and analytical perspectives, Clin. Biochem. 105–106 (2022) 1–15, https://doi.org/10.1016/J.CLINBIOCHEM.2022.04.001.
[12] S. Dayana Priyadharshini, P. Suresh Babu, S. Manikandan, R. Subbaiya, M. Govarthanan, N. Karmegam, Phycoremediation of wastewater for pollutant removal: a green approach to environmental protection and long-term remediation, Environ. Pollut. 290 (2021) 117989, https://doi.org/10.1016/J.ENVPOL.2021.117989.
[13] M. Rajabi, K. Mahanpoor, O. Moradi, Removal of dye molecules from aqueous solution by carbon nanotubes and carbon nanotube functional groups: critical review, RSC. Adv. 7 (2017) 47083–47090, https://doi.org/10.1039/c7ra09377b.
[14] S. Agarwal, I. Tyagi, V.K. Gupta, F. Golbaz, A.N. Golikand, O. Moradi, Synthesis and characteristics of polyaniline/zirconium oxide conductive nanocomposite for dye adsorption application, J. Mol. Liq. 218 (2016) 494–498, https://doi.org/10.1016/j.molliq.2016.02.040.
[15] D.A. Gkika, A.C. Mitropoulos, G.Z. Kyzas, Why reuse spent adsorbents? The latest challenges and limitations, Sci. Total Environ. 822 (2022) 153612, https://doi.org/10.1016/J.SCITOTENV.2022.153612.
[16] O. Moradi, A. Hosseinian Naeini, M.R. Kalaee, S.M.R. Mirkhan, The effect of sustainable applications of chitin and chitosan to remove dyed pollutants using adsorption: a Review, NanoNano (2023) 18, https://doi.org/10.1142/S1793292023300062.
[17] L.P. Lingamdinne, R.R. Karri, M.R. Khan, Y.-Y. Chang, J.R. Koduru, Evaluation of surface phenomena of magnetic biomass for dye removal via surface modeling, J. Environ. Chem. Eng. 9 (2021) 105953, https://doi.org/10.1016/j.jece.2021.105953.
[18] S.M. Samianifard, M. Kalaee, O. Moradi, N.M. Mahmoodi, D. Zaarei, Novel biocomposite (Starch/metal–organic framework /Graphene oxide): Synthesis, characterization and visible light assisted dye degradation, J. Photochem. Photobiol. A Chem. 450 (2024) 115417, https://doi.org/10.1016/j.jphotochem.2023.115417.
[19] N. Tripathi, Cationic and anionic dye adsorption by agricultural solid wastes: a comprehensive review, IOSR J. Appl. Chem. 5 (2017) 191–199, https://doi.org/10.2307/j.ctt46nrzt.12.
[20] O.J. N, Removal of heavy metals from sullage using activated carbon prepared from agricultural wastes, Removal of Heavy Metals… Futo Journal Series (FUTOJNLS) (2019) 219–227. www.futojnls.org.

[21] N. Tran, X. Phuong, N. Thi, T. Hong, P. Thi, K. Le, Chemically treated orange peels as a Bio-adsorbent for various dyes, 89 (2021) 79–84. https://doi.org/10.3303/CET2189014.

[22] P.M. Thabede, Sorption capacity of carbon-based mandarin orange peels for removing methylene blue and ibuprofen from water, Appl. Sci. (Switzerland) (2023) 13, https://doi.org/10.3390/app131810511.

[23] S. Ragupathy, K. Raghu, P. Prabu, Synthesis and characterization of TiO2 loaded cashew nut shell activated carbon and photocatalytic activity on BG and MB dyes under sunlight radiation, Spectrochim. Acta a Mol. Biomol. Spectrosc. (2014), https://doi.org/10.1016/j.saa.2014.11.087.

[24] A.K. Prajapati, M.K. Mondal, Comprehensive kinetic and mass transfer modeling for methylene blue dye adsorption onto CuO nanoparticles loaded on nanoporous activated carbon prepared from waste coconut shell, J. Mol. Liq. 307 (2020) 112949, https://doi.org/10.1016/j.molliq.2020.112949.

[25] R.Z. Wang, D.L. Huang, Y.G. Liu, C. Zhang, C. Lai, X. Wang, G.M. Zeng, Q. Zhang, X.M. Gong, P. Xu, Synergistic removal of copper and tetracycline from aqueous solution by steam-activated bamboo-derived biochar, J. Hazard. Mater. 384 (2020), https://doi.org/10.1016/j.jhazmat.2019.121470.

[26] B. Adsorption, Nitrogen self-doped activated carbons derived from bamboo shoots as adsorbent for methylene, (2019).

[27] G.M. Santana, P.F. Trugilho, W.M. Da Silva Borges, M.L. Bianchi, J.B. Paes, J.R. C. Nobre, R. De Medeiros Morais, Activated carbon from bamboo (bambusa vulgaris) waste using co2 as activating agent for adsorption of methylene blue and phenol, Cienc. Florest. 29 (2019) 769–778.

[28] L. Kurniawati Wulandari, S. Indra, V. Aditama, The design of filtration system using coconut shell charcoal for domestic wastewater purification, Int. J. Eng. Sci. 4 (2020) 19–23. http://ijses.com/.

[29] S. Sultana, K. Islam, M.A. Hasan, H.M.J. Khan, M.A.R. Khan, A. Deb, M. Al Raihan, M.W. Rahman, Adsorption of crystal violet dye by coconut husk powder: isotherm, kinetics and thermodynamics perspectives, Environ. Nanotechnol. Monit. Manage 17 (2022) 100651, https://doi.org/10.1016/j.enmm.2022.100651.

[30] A.M. Aljeboree, A.N. Alshirifi, A.F. Alkaim, Kinetics and equilibrium study for the adsorption of textile dyes on coconut shell activated carbon, Arab. J. Chem. 10 (2017) S3381–S3393, https://doi.org/10.1016/j.arabjc.2014.01.020.

[31] M. Qiu, L. Liu, Q. Ling, Y. Cai, S. Yu, S. Wang, D. Fu, B. Hu, X. Wang, Biochar for the removal of contaminants from soil and water: A review, Biochar. 4 (2022), https://doi.org/10.1007/s42773-022-00146-1.

[32] F.A. Adekola, S.B. Ayodele, A.A. Inyinbor, Activated biochar prepared from plaintain peels: Characterization and rhodamine B adsorption data set, Chem. Data Coll. 19 (2019), https://doi.org/10.1016/j.cdc.2018.11.012.

[33] A.O. Dada, A.A. Inyinbor, O.S. Bello, B.E. Tokula, Novel plantain peel activated carbon–supported zinc oxide nanocomposites (PPAC-ZnO-NC) for adsorption of chloroquine synthetic pharmaceutical used for COVID-19 treatment, BioMass Convers. Biorefin. (2021), https://doi.org/10.1007/s13399-021-01828-9.

[34] O.P. Abimbola, D.A. Oluwasogo, A.A. Inyinbor, Phytochemical analysis and antioxidant potential of raphia hookeri leaf and epicarp, Orient. J. Chem. 34 (2018) 2742–2746, https://doi.org/10.13005/ojc/340608.

[35] J.Q. Filipinas, K.K.P. Rivera, D.C. Ong, S.M.B. Pingul-Ong, R.R.M. Abarca, M.D. G. de Luna, Removal of sodium diclofenac from aqueous solutions by rice hull biochar, Biochar. 3 (2021) 189–200, https://doi.org/10.1007/s42773-020-00079-7.

[36] T. Mukoko, M. Mupa, U. Guyo, F. Dziike, Preparation of rice hull activated carbon for the removal of selected pharmaceutical waste compounds in hospital effluent, Environ. Anal. Toxicol. (2015), https://doi.org/10.4172/2161-0525.S7-008.

[37] H.N. Bhatti, A. Jabeen, M. Iqbal, S. Noreen, Z. Naseem, Adsorptive behavior of rice bran-based composites for malachite green dye: Isotherm, kinetic and thermodynamic studies, J. Mol. Liq. 237 (2017) 322–333, https://doi.org/10.1016/j.molliq.2017.04.033.

[38] P.M. Thabede, N.A.H. Khumalo, P.N. Mahlambi, P. Nyamukamba, S.J. Modise, Sorption of Ibuprofen by chemically treated maize cob, S. Afr. J. Chem. Eng. 46 (2023) 376–385, https://doi.org/10.1016/j.sajce.2023.09.002.

[39] G. Adebayo, H. Adegoke, W. Jamiu, B. Balogun, A. Jimoh, Adsorption of Mn(II) and Co(II) ions from aqueous solution using Maize cob activated carbon: Kinetics and thermodynamics studies, J. Appl. Sci. Environ. Manage. 19 (2016) 737, https://doi.org/10.4314/jasem.v19i4.22.

[40] C. Afmc, J.O. Ojediran, A.O. Dada, S.O. Aniyi, R.O. David, A.D. Adewumi, Mechanism and isotherm modeling of effective adsorption of malachite green as endocrine disruptive dye using Acid Functionalized Maize, Sci. Rep. (2021) 1–15, https://doi.org/10.1038/s41598-021-00993-1.

[41] Aruna, N.Bagotia, A.K. Sharma, S. Kumar, A review on modified sugarcane bagasse biosorbent for removal of dyes, ChemosphereChemosphere 268 (2021). https://doi.org/10.1016/j.chemosphere.2020.129309.

[42] S. Mustefa, S.V. Prabhu, T.T. Sissay, A.A. Getahun, Sugarcane bagasse based activated carbon preparation and its adsorption efficacy on removal of BOD and COD from textile effluents : RSM based modeling, optimization and kinetic aspects, Bioresour. Technol. Rep. 14 (2021) 100664, https://doi.org/10.1016/j.biteb.2021.100664.

[43] M. Hassan, R. Naidu, J. Du, Y. Liu, F. Qi, Critical review of magnetic biosorbents: Their preparation, application, and regeneration for wastewater treatment, Sci. Total Environ. 702 (2020) 134893, https://doi.org/10.1016/J.SCITOTENV.2019.134893.

[44] L. Liang, F. Xi, W. Tan, X. Meng, B. Hu, X. Wang, Review of organic and inorganic pollutants removal by biochar and biochar-based composites, Biochar. 3 (2021) 255–281, https://doi.org/10.1007/s42773-021-00101-6.

[45] J. Xiong, M. Zhou, C. Qu, D. Yu, C. Chen, M. Wang, W. Tan, Quantitative analysis of Pb adsorption on sulfhydryl-modified biochar, Biochar. 3 (2021) 37–49, https://doi.org/10.1007/s42773-020-00077-9.

[46] M. Movva, R. Kommineni, Effect of green gram husk nanocellulose on banana fiber composite effect of green gram husk nanocellulose on banana fiber, J. Nat. Fibers 00 (2017) 1–13, https://doi.org/10.1080/15440478.2017.1414658.

[47] O.S. Agboola, O.S. Bello, Enhanced adsorption of ciprofloxacin from aqueous solutions using functionalized banana stalk, (2020).

[48] E. Misran, O. Bani, E.M. Situmeang, A.S. Purba, Banana stem based activated carbon as a low-cost adsorbent for methylene blue removal: Isotherm, kinetics, and reusability, Alex. Eng. J. 61 (2022) 1946–1955, https://doi.org/10.1016/j.aej.2021.07.022.

[49] S.F.M. Hanafiah, N.F.M. Salleh, N.A. Ghafar, N.M. Shukri, N.H.N. Kamarudin, M. Hapani, R. Jusoh, Efficiency of coconut husk as agricultural adsorbent in removal of chromium and nickel ions from aqueous solution, IOP. Conf. Ser. Earth. Environ. Sci. 596 (2020), https://doi.org/10.1088/1755-1315/596/1/012048.

[50] O.S. Bello, M.A. Moshood, B.A. Ewetumo, I.C. Afolabi, Ibuprofen removal using coconut husk activated Biomass, Chem. Data Coll. 29 (2020) 1–10, https://doi.org/10.1016/j.cdc.2020.100533.

[51] T. Halfhide, L.J. Lalgee, K.S. Singh, J. Williams, M. Sealy, A. Manoo, A. Mohammed, Nutrient removal using spent coconut husks, H2Open J. 2 (2019) 125–136, https://doi.org/10.2166/H2OJ.2019.011.

[52] S. Montoya-Suarez, F. Colpas-Castillo, E. Meza-Fuentes, J. Rodríguez-Ruiz, R. Fernandez-Maestre, Activated carbons from waste of oil-palm kernel shells, sawdust and tannery leather scraps and application to chromium (VI), phenol, and methylene blue dye adsorption, Water Sci. Technol. 73 (2016) 21–27, https://doi.org/10.2166/wst.2015.293.

[53] Cd (II) and Ni (II) uptake by novel biosorbent prepared from oil palm residual biomass and Al 2 O 3 nanoparticles, 15 (2020). https://doi.org/10.1016/j.scp.2020.100216.

[54] H. Wang, C. Fang, Q. Wang, Y. Chu, Y. Song, Y. Chen, X. Xue, Sorption of tetracycline on biochar derived from rice straw and swine manure, RSC. Adv. 8 (2018) 16260–16268, https://doi.org/10.1039/c8ra01454j.

[55] N.T. Luyen, H.X. Linh, T.Q. Huy, Preparation of rice husk biochar-based magnetic nanocomposite for effective removal of crystal violet, J. Electron. Mater. 49 (2020) 1142–1149, https://doi.org/10.1007/s11664-019-07798-z.

[56] M. Ulfah, S. Raharjo, P. Hastuti, P. Darmadji, The potential of palm kernel shell activated carbon as an adsorbent for β- carotene recovery from crude palm oil, Advances of science and technology for, Society.Society. 130016 (2018) 1–6, https://doi.org/10.1063/1.4958560.

[57] Y. Miyah, A. Lahrichi, M. Idrissi, Removal of cationic dye – Methylene bleu – from aqueous solution by adsorption onto corn cob powder calcined, J. Mater. Environ. Sci 7 (2016) 96–104.

[58] N. Kannan, A. Vijayakumar, P. Subramaniam, Studies on the removal of red industrial dye using teak leaf, Maize Corn and Babool Tree Bark Carbons – A Comparison 7 (2010) 770–774.

[59] A.A. Wani, A.M. Khan, Y.K. Manea, M.A.S. Salem, M. Shahadat, Selective adsorption and ultrafast fluorescent detection of Cr(VI) in wastewater using neodymium doped polyaniline supported layered double hydroxide nanocomposite, J. Hazard. Mater. 416 (2021) 125754, https://doi.org/10.1016/j.jhazmat.2021.125754.

[60] Z. Zhao, B. Wang, B.K.G. Theng, X. Lee, X. Zhang, M. Chen, P. Xu, Removal performance, mechanisms, and influencing factors of biochar for air pollutants: A critical review, Biochar. 4 (2022), https://doi.org/10.1007/s42773-022-00156-z.

[61] D. Robati, B. Mirza, M. Rajabi, O. Moradi, I. Tyagi, S. Agarwal, V.K. Gupta, Removal of hazardous dyes-BR 12 and methyl orange using graphene oxide as an adsorbent from aqueous phase, J. Chem. Eng. 284 (2016) 687–697, https://doi.org/10.1016/j.cej.2015.08.131.

[62] D. Robati, M. Rajabi, O. Moradi, F. Najafi, I. Tyagi, S. Agarwal, V.K. Gupta, Kinetics and thermodynamics of malachite green dye adsorption from aqueous solutions on graphene oxide and reduced graphene oxide, J. Mol. Liq. 214 (2016) 259–263, https://doi.org/10.1016/j.molliq.2015.12.073.

[63] R.A. Rashid, A.H. Jawad, M.A.M. Ishak, N.N. Kasim, KOH-activated carbon developed from biomass waste: adsorption equilibrium, kinetic and thermodynamic studies for Methylene blue uptake, Desalin. Water Treat 57 (2016) 27226–27236, https://doi.org/10.1080/19443994.2016.1167630.

[64] Y. Gao, Q. Yue, B. Gao, A. Li, Insight into activated carbon from different kinds of chemical activating agents: A review, Sci. Total Environ. 746 (2020) 141094, https://doi.org/10.1016/j.scitotenv.2020.141094.

[65] L. Leng, Q. Xiong, L. Yang, H. Li, Y. Zhou, W. Zhang, S. Jiang, H. Li, H. Huang, An overview on engineering the surface area and porosity of biochar, Sci. Total Environ. 763 (2021) 144204, https://doi.org/10.1016/J.SCITOTENV.2020.144204.

[66] T. Adekanye, O. Dada, J. Kolapo, Pyrolysis of maize cob at different temperatures for biochar production: Proximate, ultimate and spectroscopic characterisation, J. Agric. Eng. 68 (2022) 27–34, https://doi.org/10.17221/106/2020-RAE.

[67] M. Lutfi, Hanafi, B.Susilo, J. Prasetyo, Sandra, U.Prajogo, Characteristics of activated carbon from coconut shell (Cocos nucifera) through chemical activation process, IOP. Conf. Ser. Earth. Environ. Sci. 733 (2021). https://doi.org/10.1088/1755-1315/733/1/012134.

[68] A. Nyamful, E.K. Nyogbe, L. Mohammed, M.N. Zainudeen, S.A. Darkwa, I. Phiri, M. Mohammed, J.M. Ko, Processing and characterization of activated carbon from coconut shell and palm kernel shell waste by H3PO4 activation, Ghana J Sci 61 (2021) 91–104, https://doi.org/10.4314/gjs.v61i2.9.

[69] A.H. Jawad, M. Bardhan, M.A. Islam, M.A. Islam, S.S.A. Syed-Hassan, S.N. Surip, Z.A. ALOthman, M.R. Khan, Insights into the modeling, characterization and adsorption performance of mesoporous activated carbon from corn cob residue via microwave-assisted H3PO4 activation, Surf. Interfaces. 21 (2020) 100688, https://doi.org/10.1016/j.surfin.2020.100688.

[70] M. Azmier, N. Azreen, A. Puad, O. Solomon, Kinetic, equilibrium and thermodynamic studies of synthetic dye removal using pomegranate peel activated carbon prepared by microwave-induced KOH activation, Water Resour Ind 6 (2014) 18–35, https://doi.org/10.1016/j.wri.2014.06.002.

[71] O.S. Bello, K.A. Adegoke, A.A. Inyinbor, A.O. Dada, Trapping Rhodamine B dye using functionalized mango (Mangifera indica) pod, Water Environ. Res. 93 (2021) 2308–2328, https://doi.org/10.1002/wer.1606.

[72] T. Luo, C. Luo, Z. Shi, X. Li, F. Wu, L. Zhang, Optimization of sol–gel combustion synthesis of calcium looping CO2 sorbents, Part II: Effects of thermal activation conditions, Sep. Purif. Technol. 292 (2022) 121061, https://doi.org/10.1016/J.SEPPUR.2022.121061.

[73] Y.X. Seow, Y.H. Tan, N.M. Mubarak, J. Kansedo, M. Khalid, M.L. Ibrahim, M. Ghasemi, A review on biochar production from different biomass wastes by recent carbonization technologies and its sustainable applications, J. Environ. Chem. Eng. 10 (2022) 107017, https://doi.org/10.1016/J.JECE.2021.107017.

[74] P.T. Lum, K.Y. Foo, N.A. Zakaria, P. Palaniandy, Ash based nanocomposites for photocatalytic degradation of textile dye pollutants: A review, Mater. Chem. Phys. (2020) 241, https://doi.org/10.1016/j.matchemphys.2019.122405.

[75] G. Das, H.S. Shin, A. Kumar, C.N. Vishnuprasad, J.K. Patra, Photo-mediated optimized synthesis of silver nanoparticles using the extracts of outer shell fibre of Cocos nucifera L. fruit and detection of its antioxidant, cytotoxicity and antibacterial potential, Saudi. J. Biol. Sci. 28 (2021) 980–987, https://doi.org/10.1016/j.sjbs.2020.11.022.

[76] R. V, S. G, A. R, B. S, Synthesis of Zinc Oxide nanoparticles and setariaverticillata assisted activated carbon blended Zinc Oxide nanoparticles, Indian J Sci Technol 12 (2019) 1–6, https://doi.org/10.17485/ijst/2019/v12i37/147468.

[77] M.M. Chikkanna, S.E. Neelagund, K.K. Rajashekarappa, Green synthesis of Zinc oxide nanoparticles (ZnO NPs) and their biological activity, SN. Appl. Sci. 1 (2019) 1–10, https://doi.org/10.1007/s42452-018-0095-7.

[78] A. Ali, S.S.R. Koloor, A.H. Alshehri, A. Arockiarajan, Carbon nanotube characteristics and enhancement effects on the mechanical features of polymer-based materials and structures- A review., 24, 6495 –6521, J. Mater. Res. Technol. 24 (2023) 6495–6521.

[79] M. Vinyas, S.J. Athul, D. Harursampath, M. Loja, T.Nguyen Thoi, A comprehensive review on analysis of nanocomposites: From manufacturing to properties characterization, Mater. Res. Express. 6 (2019). https://doi.org/10.1088/2053-1591/ab3175.

[80] A.V. Rane, K. Kanny, V.K. Abitha, S. Thomas, Methods for synthesis of nanoparticles and fabrication of nanocomposites, in: Synthesis of inorganic nanomaterials, Elsevier (2018) 121–139, https://doi.org/10.1016/b978-0-08-101975-7.00005-1.

[81] D. Coetzee, M. Venkataraman, J. Militky, M. Petru, Influence of nanoparticles on thermal and electrical conductivity of composites, Polymers. (Basel) 12 (2020) 1–25, https://doi.org/10.3390/POLYM12040742.

[82] S.K. Parida, Polymer nanocomposites and applications: A brief review, Int. J. Sci. Res. Phys. Appl. Sci. 6 (2020) 75–78, https://doi.org/10.26438/ijsrpas/v6i3.7578.

[83] H.T. Van, T.M.P. Nguyen, V.T. Thao, X.H. Vu, T.V. Nguyen, L.H. Nguyen, Applying activated carbon derived from coconut shell loaded by silver nanoparticles to remove methylene blue in aqueous solution, Water. Air. Soil. Pollut. 229 (2018), https://doi.org/10.1007/s11270-018-4043-3.

[84] B.T. Atunwa, A.O. Dada, A.A. Inyinbor, U. Pal, Synthesis, physiochemical and spectroscopic characterization of palm kernel shell activated carbon doped AgNPs (PKSAC@AgNPs) for adsorption of chloroquine pharmaceutical waste, Mater. Today Proc. 65 (2022) 3538–3546, https://doi.org/10.1016/j.matpr.2022.06.099.

[85] J. Dhanalakshmi, D.P. Padiyan, Photocatalytic degradation of methyl orange and bromophenol blue dyes in water using sol-gel synthesized TiO2 nanoparticles, Mater. Res. Express. 4 (2017), https://doi.org/10.1088/2053-1591/aa85fd.

[86] M. Pudukudy, Z. Yaakob, M.Z. Mazuki, M.S. Takriff, S.S. Jahaya, One-pot sol-gel synthesis of MgO nanoparticles supported nickel and iron catalysts for undiluted methane decomposition into COx free hydrogen and nanocarbon, Appl. Catal. B (2017), https://doi.org/10.1016/j.apcatb.2017.04.070.

[87] K. Kaviyarasu, E. Manikandan, J. Kennedy, M. Jayachandran, M. Maaza, Rice husks as a sustainable source of high quality nanostructured silica for high performance Li-ion battery requital by sol-gel method – a review, Adv. Materials Letters 7 (2016) 684–696, https://doi.org/10.5185/amlett.2016.6192.

[88] A.H. Jawad, U.K. Sahu, M.S. Mastuli, Z.A. ALOthman, L.D. Wilson, Multivariable optimization with desirability function for carbon porosity and methylene blue adsorption by watermelon rind activated carbon prepared by microwave assisted H3PO4, BioMass Convers. Biorefin. 14 (2024) 577–591, https://doi.org/10.1007/s13399-022-02423-2.

[89] A.H. Jawad, Z.S. Mehdi, M.A.M. Ishak, K. Ismail, Large surface area activated carbon from low-rank coal via microwave-assisted KOH activation for methylene blue adsorption, Desalin. Water Treat 110 (2018) 239–249, https://doi.org/10.5004/dwt.2018.22226.

[90] R. Atchudan, T.N. Jebakumar Immanuel Edison, M. Shanmugam, S. Perumal, T. Somanathan, Y.R. Lee, Sustainable synthesis of carbon quantum dots from banana peel waste using hydrothermal process for in vivo bioimaging, Physica e Low. Dimens. Syst. Nanostruct. 126 (2021) 114417, https://doi.org/10.1016/j.physe.2020.114417.

[91] R. Atchudan, T. Nesakumar, J. Immanuel, M. Shanmugam, S. Perumal, T. Somanathan, Y. Rok, E. Physica, Low-dimensional Systems and Nanostructures Sustainable synthesis of carbon quantum dots from banana peel waste using hydrothermal process for in vivo bioimaging ☆, Physica e Low. Dimens. Syst. Nanostruct. 126 (2021) 114417 https://doi.org/10.1016/j.physe.2020.114417.

[92] N. Sankararamakrishnan, N. Singh, I. Srivastava, Hierarchical nano Fe(0)@FeS doped cellulose nanofibres derived from agrowaste – Potential bionanocomposite for treatment of organic dyes, Int. J. Biol. Macromol. 151 (2020) 713–722, https://doi.org/10.1016/j.ijbiomac.2020.02.155.

[93] A.M. Abdel-Wahab, A.S. Al-Shirbini, O. Mohamed, O. Nasr, Photocatalytic Degradation of Paracetamol Over Magnetic Flower-Like TiO2/Fe2O3 Core-Shell Nanostructures, Elsevier B.V., 2017, https://doi.org/10.1016/j.jphotochem.2017.07.030.

[94] A.O. Dada, F.A. Amoo, E.F. Dada, A.T. Adelani-akande, O.M. Bello, R. C. Okonkwo, A.A. Iyinbor, P.A. Abimbola, O. Adeniyi, O.A. Kolawole, O. C. Adewunmi, Silver nanoparticle synthesis by Acalypha wilkesiana extract : phytochemical screening, characterization, influence of operational parameters, and preliminary antibacterial testing, Heliyon. 5 (2019) 1–8, https://doi.org/10.1016/j.heliyon.2019.e02517.

[95] X. Hu, Y. Li, Y. Xu, Z. Gan, X. Zou, J. Shi, X. Huang, Green one-step synthesis of carbon quantum dots from orange peel for fluorescent detection of Escherichia coli in milk, Food Chem. 339 (2021) 127775, https://doi.org/10.1016/j.foodchem.2020.127775.

[96] A. Herrera-Barros, C. Tejada-Tovar, A. Villabona-Ortíz, A. González-Delgado, R. Mejiá-Meza, Assessment of the effect of AL2O3 and TIO2 nanoparticles on orange peel biomass and its application for CD (II) and Ni (II) uptake, Trans. ASABe 62 (2019) 139–147, https://doi.org/10.13031/trans.12966.

[97] Y. Phang, M. Aminuzzaman, G. Muhammad, S. Ogawa, A. Watanabe, L.-H. Tey, 1, Green synthesis and characterization of CuO nanoparticles derived from papaya peel extract for the photocatalytic degradation of palm oil mill effluent (POME), Sustainability. 13 (2021) 796, https://doi.org/10.3390/su13020796.

[98] R. Zhang, Z. Wang, Z. Zhou, D. Li, T. Wang, P. Su, Y. Yang, Highly effective removal of pharmaceutical compounds from aqueous solution by magnetic Zr-based MOFs composites, Ind. Eng. Chem. Res. 58 (2019) 3876–3884, https://doi.org/10.1021/acs.iecr.8b05244.

[99] G. López-téllez, C.E. Barrera-díaz, P. Balderas-hernández, G. Roa-morales, B. Bilyeu, Removal of hexavalent chromium in aquatic solutions by iron nanoparticles embedded in orange peel pith, 173 (2011) 480–485. https://doi.org/10.1016/j.cej.2011.08.018.

[100] S. Zhang, X. Lu, Treatment of wastewater containing reactive brilliant blue KN-R using TiO_2/BC composite as heterogeneous photocatalyst and adsorbent, ChemosphereChemosphere (2018), https://doi.org/10.1016/j.chemosphere.2018.05.073.

[101] A.M. El-Saeed, M.A. El-Fattah, A.M. Azzam, Synthesis of ZnO nanoparticles and studying its influence on the antimicrobial, anticorrosion and mechanical behavior of polyurethane composite for surface coating, Dyes and Pigm. 121 (2015) 282–289, https://doi.org/10.1016/j.dyepig.2015.05.037.

[102] A. Herrera-Barros, C. Tejada-Tovar, A. Villabona-Ortíz, A. González-Delgado, R. Mejía-Meza, Assessment of the effect of Al2O3 and TiO2 nanoparticles on orange peel biomass and its application for Cd (II) and Ni (II) uptake, ASABE 62 (2019) 139–147.

[103] T. Uyen, D. Thi, T. Nguyen, Y.D. Thi, H. Ta, Green synthesis of ZnO nanoparticles using orange fruit peel extract for antibacterial activities, (2020) 23899–23907. https://doi.org/10.1039/d0ra04926c.

[104] K.G. Raj, P.A. Joy, Coconut shell based activated carbon-iron oxide magnetic nanocomposite for fast and efficient removal of oil spills, J. Environ. Chem. Eng. 3 (2015) 2068–2075, https://doi.org/10.1016/j.jece.2015.04.028.

[105] Z. Saadati, M. Gilani, Kinetics, isotherms, and thermodynamic modeling of liquid-phase adsorption of Rhodamine B dye onto Fe/ZnO-shrimp shell nanocomposite, Desalin. Water Treat 85 (2018) 175–183, https://doi.org/10.5004/dwt.2017.21070.

[106] J. Adorna, M. Borines, V.D. Dang, R. Doong, Coconut shell derived activated biochar – manganese dioxide nanocomposites for high performance capacitive deionization, Desalin.. 492 (2020) 114602, https://doi.org/10.1016/j.desal.2020.114602.

[107] Z. Hao, C. Wang, Z. Yan, H. Jiang, H. Xu, Magnetic particles modification of coconut shell-derived activated carbon and biochar for effective removal of phenol from water, ChemosphereChemosphere 211 (2018) 1–30, https://doi.org/10.1016/j.chemosphere.2018.08.038.

[108] D.A. Oluwasogo, S. Varangane, Y.T. Prabhu, B.M. Abraham, V. Perupogu, U, Pal, Biosynthetic modulation of carbon-doped ZnO for rapid photocatalytic endocrine disruptive remediation and hydrogen evolution, J. Clean. Prod. 394 (2023), https://doi.org/10.1016/j.jclepro.2023.136393.

[109] A. Rehman, S. Farrukh, A. Hussain, E. Pervaiz, Synthesis and effect of metal–organic frame works on CO2 adsorption capacity at various pressures: A contemplating review, Energy and Environment (2019), https://doi.org/10.1177/0958305X19865352.

[110] S. Dutta, B. Gupta, S.K. Srivastava, A.K. Gupta, Recent advances on the removal of dyes from wastewater using various adsorbents: a critical review, Mater. Adv. 2 (2021) 4497–4531, https://doi.org/10.1039/d1ma00354b.

[111] Y. Zhu, W.H. Fan, W.Y. Feng, Y. Wang, S. Liu, Z.M. Dong, X.M. Li, A critical review on metal complexes removal from water using methods based on Fenton-like reactions: Analysis and comparison of methods and mechanisms, J. Hazard. Mater. 414 (2021), https://doi.org/10.1016/j.jhazmat.2021.125517.

[112] V. Katheresan, J. Kansedo, S.Y. Lau, Efficiency of various recent wastewater dye removal methods: A review, J. Environ. Chem. Eng. 6 (2018) 4676–4697, https://doi.org/10.1016/j.jece.2018.06.060.
[113] X.P. Liu, M.H. Zhang, J.Y. Feng, L.F. Yang, P.J. Zhang, Removal of trace antibiotics from wastewater: a systematic study of nanofiltration combined with ozone based advanced oxidation processes, Chem. Eng. J. 240 (2014) 211.
[114] B. Farahani, M. Giahi, M.H. Ghorbani, R. Fazaeli, O. Moradi, Synthesis of CuS/NiS heterostructural photocatalyst and its performance in the degradation of metronidazole and diclofenac drugs: Optimization of operating conditions, J. Nanostructure Chem. 13 (2023) 303–320, https://doi.org/10.1007/s40097-022-00520-2.
[115] O. Moradi, I.Daneshmand Sharabaf, Separation of organic contaminant (dye) using the modified porous metal-organic framework (MIL), Environ. Res. 214 (2022). https://doi.org/10.1016/j.envres.2022.114006.
[116] L. Sellaoui, A. Gómez-Avilés, F. Dhaouadi, J. Bedia, A. Bonilla-Petriciolet, S. Rtimi, C. Belver, Adsorption of emerging pollutants on lignin-based activated carbon: Analysis of adsorption mechanism via characterization, kinetics and equilibrium studies, J. Chem. Eng. 452 (2023), https://doi.org/10.1016/j.cej.2022.139399.
[117] D.T. Bankole, A.P. Oluyori, A.A. Inyinbor, Acid-activated Hibiscus sabdariffa seed pods biochar for the adsorption of Chloroquine phosphate: Prediction of adsorption efficiency via machine learning approach, S. Afr. J. Chem. Eng. 42 (2022) 162–175, https://doi.org/10.1016/j.sajce.2022.08.012.
[118] K. Intarasuwan, P. Amornpitoksuk, S. Suwanboon, P. Graidist, S. Maungchanburi, C. Randorn, Effect of Ag loading on activated carbon doped ZnO for bisphenol A degradation under visible light, Adv. Powder Technol. 29 (2018) 2608–2615, https://doi.org/10.1016/J.APT.2018.07.006.
[119] O. Moradi, M.A. Madanpisheh, M. Moghaddas, Synthesis of GO/HEMA, GO/HEMA/TiO2, and GO/Fe3O4/HEMA as novel nanocomposites and their dye removal ability, Adv. Compos. Hybrid. Mater. 4 (2021) 1185–1204, https://doi.org/10.1007/s42114-021-00353-7.
[120] O.S. Bello, B.M. Lasisi, O.J. Adigun, V. Ephraim, Scavenging Rhodamine B dye using moringa oleifera seed pod, Chem. Speciation Bioavailability 29 (2017) 120–134, https://doi.org/10.1080/09542299.2017.1356694.
[121] A.O. Dada, F.A. Adekola, E.O. Odebunmi, Kinetics, mechanism, isotherm and thermodynamic studies of liquid-phase adsorption of Pb2+ onto wood activated carbon supported zerovalent iron (WAC-ZVI) nanocomposite, Cogent. Chem. (2017) 68, https://doi.org/10.1080/23312009.2017.1351653.
[122] P.R. Gawande, J. Kaware, Characterization and activation of coconut shell activated carbon research paper, Int. J. Eng. Sci. Invention 6 (2017) 43–49. www.ijesi.org.
[123] O.A. Ekpete, A.C. Marcus, V. Osi, Preparation and characterization of activated carbon obtained from plantain (Musa paradisiaca) fruit stem, J. Chem. (2017) 2017, https://doi.org/10.1155/2017/8635615.
[124] K.K. Katibi, K.F. Yunos, H.C. Man, A.Z. Aris, M.Z.M. Nor, R.S. Azis, An insight into a sustainable removal of bisphenol a from aqueous solution by novel palm kernel shell magnetically induced biochar: Synthesis, characterization, kinetic, and thermodynamic studies, Polymers. (Basel) (2021) 13, https://doi.org/10.3390/polym13213781.
[125] M.O. Bello, N. Abdus-Salam, F.A. Adekola, U. Pal, Isotherm and kinetic studies of adsorption of methylene blue using activated carbon from ackee apple pods, Chem. Data Coll. (2021) 31, https://doi.org/10.1016/j.cdc.2020.100607.
[126] A. Elavarasan, S. Chitradevi, V. Nandhakumar, S. Sivajiganesan, S. Kadhiravan, FT-IR Spectra, XRD and EDX Studies on the adsorption of methylene blue dye present in aqueous solution onto acid activated carbon prepared from mimusops elengi leaves, J. Appl. Chem. 11 (2018) 45–51, https://doi.org/10.9790/5736-1107034551.
[127] O. Moradi, A. Pudineh, S. Sedaghat, Synthesis and characterization Agar/GO/ZnO NPs nanocomposite for removal of methylene blue and methyl orange as azo dyes from food industrial effluents, Food Chem. Toxicol. 169 (2022), https://doi.org/10.1016/j.fct.2022.113412.
[128] A.H. Jawad, S.E.M. Saber, A.S. Abdulhameed, A. Reghioua, Z.A. ALOthman, L. D. Wilson, Mesoporous activated carbon from mangosteen (Garcinia mangostana) peels by H3PO4 assisted microwave: Optimization, characterization, and adsorption mechanism for methylene blue dye removal, Diam. Relat. Mater. 129 (2022), https://doi.org/10.1016/j.diamond.2022.109389.
[129] M. Kaya, Preparation and TG /DTG, FT-IR, SEM, BET Surface Area, Iodine Number and Methylene Blue Number Analysis of Activated Carbon from Pistachio Shells by Chemical Activation (2017) 1–13, https://doi.org/10.1515/ijcre-2017-0060.
[130] K.S. Obayomi, A.E. Oluwadiya, S.Y. Lau, A.O. Dada, D. Akubuo-Casmir, T. A. Adelani-Akande, A.S.M. Fazle Bari, S.O. Temidayo, M.M. Rahman, Biosynthesis of Tithonia diversifolia leaf mediated Zinc Oxide Nanoparticles loaded with flamboyant pods (Delonix regia) for the treatment of Methylene Blue Wastewater, Arab. J. Chem. 14 (2021) 103363, https://doi.org/10.1016/J.ARABJC.2021.103363.
[131] K. Jurkiewicz, M. Pawlyta, A. Burian, Structure of carbon materials explored by local transmission electron microscopy and global powder diffraction probes, C. (Basel) 4 (2018) 68, https://doi.org/10.3390/c4040068.
[132] K.S. Bhavsar, P.K. Labhane, R.B. Dhake, G.H. Sonawane, Crystal structures, morphological, optical, adsorption, kinetic and photocatalytic degradation studies of activated carbon loaded BiOBr nanoplates prepared by solvothermal method, Inorg. Chem. Commun. 104 (2019) 134–144, https://doi.org/10.1016/j.inoche.2019.04.002.
[133] S. Daniel, Chapter 4 - Characterization of carbon dots, Editor(s): Suresh Kumar Kailasa, Chaudhery Mustansar Hussain, Carbon Dots in Analytical Chemistry (2023), https://doi.org/10.1016/B978-0-323-98350-1.00015-3.
[134] A. Ali, S. Saeid, R. Koloor, A.H. Alshehri, Carbon nanotube characteristics and enhancement effects on the mechanical features of polymer- based materials and structures e A review, J. Mater. Res. Technol. 24 (2023) 6495–6521, https://doi.org/10.1016/j.jmrt.2023.04.072.
[135] Y. Wang, H. Wang, X. Wang, Y. Xiao, Y. Zhou, X. Su, J. Cai, F. Sun, Resuscitation, isolation and immobilization of bacterial species for efficient textile wastewater treatment: A critical review and update, Sci. Total Environ. 730 (2020) 139034, https://doi.org/10.1016/J.SCITOTENV.2020.139034.
[136] A. Tkaczyk, K. Mitrowska, A. Posyniak, Synthetic organic dyes as contaminants of the aquatic environment and their implications for ecosystems: A review, Sci. Total Environ. 717 (2020) 137222, https://doi.org/10.1016/J.SCITOTENV.2020.137222.
[137] S. Samsami, M. Mohamadi, M.H. Sarrafzadeh, E.R. Rene, M. Firoozbahr, Recent advances in the treatment of dye-containing wastewater from textile industries: Overview and perspectives, Process Saf. Environ. Prot. 143 (2020) 138–163, https://doi.org/10.1016/j.psep.2020.05.034.
[138] M.M. Hassan, C.M. Carr, Biomass-derived porous carbonaceous materials and their composites as adsorbents for cationic and anionic dyes: A review, ChemosphereChemosphere 265 (2021), https://doi.org/10.1016/j.chemosphere.2020.129087.
[139] M. Hasanzadeh, A. Simchi, H.S. Far, Kinetics and adsorptive study of organic dye removal using water-stable nanoscale metal organic frameworks, Mater. Chem. Phys. 233 (2019) 267–275, https://doi.org/10.1016/j.matchemphys.2019.05.050.
[140] M. Goswami, P. Phukan, Enhanced adsorption of cationic dyes using sulfonic acid modified activated carbon, J. Environ. Chem. Eng. 5 (2017) 3508–3517, https://doi.org/10.1016/j.jece.2017.07.016.
[141] M. Mehrabi, V. Javanbakht, Photocatalytic degradation of cationic and anionic dyes by a novel nanophotocatalyst of TiO2/ZnTiO3/αFe2O3 by ultraviolet light irradiation, J. Mater. Sci.: Mater. Electron. 29 (2018) 9908–9919, https://doi.org/10.1007/s10854-018-9033-0.
[142] J. Zhang, F. Li, Q. Sun, Rapid and selective adsorption of cationic dyes by a unique metal-organic framework with decorated pore surface, Appl. Surf. Sci. 440 (2018) 1219–1226, https://doi.org/10.1016/j.apsusc.2018.01.258.
[143] N.C. Corda, M.S. Kini, A Review on adsorption of cationic dyes using activated carbon, MATEC Web Conf. 144 (2018) 02022, https://doi.org/10.1051/matecconf/201814402022.
[144] D.S. Kharat, Preparing agricultural residue based adsorbents for the removal of dyes from effluents- A review, Braz. J. Chem. Eng. 32 (2015) 1–12.
[145] F. Bouaziz, M. Koubaa, F. Kallel, R.E. Ghorbel, S.E. Chaabouni, Adsorptive removal of malachite green from aqueous solutions by almond gum: Kinetic study and equilibrium isotherms, Int. J. Biol. Macromol. 105 (2017) 56–65, https://doi.org/10.1016/j.ijbiomac.2017.06.106.
[146] A.A. Inyinbor, F.A. Adekola, G.A. Olatunji, Kinetics, isotherms and thermodynamic modeling of liquid phase adsorption of Rhodamine B dye onto Raphia hookerie fruit epicarp, Water Resour Ind 15 (2016) 14–27, https://doi.org/10.1016/j.wri.2016.06.001.
[147] A.A. Inyinbor, F.A. Adekola, G.A. Olatunji, Liquid phase adsorptions of Rhodamine B dye onto raw and chitosan supported mesoporous adsorbents: isotherms and kinetics studies, Appl. Water. Sci. 7 (2016) 2297–2307, https://doi.org/10.1007/s13201-016-0405-4.
[148] G.B. Adebayo, J. Wasiu, O.O. Oluwasina, A. Abiodun, Adsorption of crystal violet dye from aqueous solution onto activated carbon prepared from palm kernel shell, TechConnect Briefs 2018 - Advanced Materials 1 (2018) 200–203.
[149] S. Shakoor, A. Nasar, Utilization of cucumis sativus peel as an Eco-friendly biosorbent for the confiscation of crystal violet dye from artificially contaminated wastewater, Anal. Chem. Lett. 9 (2019) 1–19, https://doi.org/10.1080/22297928.2019.1588162.
[150] A.M. Rabie, M.R. Abukhadra, A.M. Rady, S.A. Ahmed, A. Labena, H.S. H. Mohamed, M.A. Betiha, J.J. Shim, Instantaneous photocatalytic degradation of malachite green dye under visible light using novel green Co–ZnO/algae composites, Res. Chem. Intermed. 46 (2020) 1955–1973, https://doi.org/10.1007/s11164-019-04074-x.
[151] D. Lin, F. Wu, Y. Hu, T. Zhang, C. Liu, Q. Hu, Y. Hu, Z. Xue, H. Han, T. Ko, Adsorption of Dye by Waste Black Tea Powder : Parameters, kinetic, equilibrium, and thermodynamic studies, J. Chem. 2020 (2020) 1–11.
[152] A. Bazan-Wozniak, A. Nosal-Wiercińska, S. Yilmaz, R. Pietrzak, Chitin-based porous carbons from Hermetia illucens fly with large surface area for efficient adsorption of methylene blue; adsorption mechanism, kinetics and equilibrium studies, Measurement. (Lond) (2024) 226, https://doi.org/10.1016/j.measurement.2024.114129.
[153] A.O. Dada, F.A. Adekola, E.O. Odebunmi, F.E. Dada, O.S. Bello, A.S. Ogunlaja, Bottom-up approach synthesis of core-shell nanoscale zerovalent iron (CS-nZVI): physicochemical and spectroscopic characterization with Cu(II) ions adsorption application, MethodsX.MethodsX. 7 (2020), https://doi.org/10.1016/j.mex.2020.100976.
[154] O.A. Dada, F.A. Adekola, E.O. Odebunmi, Kinetics and equilibrium models for sorption of Cu(II) onto a novel manganese nano-adsorbent, J. Dispers. Sci. Technol. 37 (2016) 119–133, https://doi.org/10.1080/01932691.2015.1034361.
[155] C. Leodopoulos, D. Doulia, K. Gimouhopoulos, Adsorption of cationic dyes onto bentonite, Sep. Purif. Rev. 44 (2014) 74–107, https://doi.org/10.1080/15422119.2013.823622.

[156] Z. Wu, X. Yuan, H. Zhong, H.H. Wang, G. Zeng, X. Chen, H.H. Wang, L. Zhang, J. Shao, Enhanced adsorptive removal of p-nitrophenol from water by aluminum metal-organic framework/reduced graphene oxide composite, Sci. Rep. 6 (2016) 1–13, https://doi.org/10.1038/srep25638.
[157] M. Sarker, I. Ahmed, S.H. Jhung, Adsorptive removal of herbicides from water over nitrogen-doped carbon obtained from ionic liquid@ZIF-8, J. Chem. Eng. 323 (2017) 203–211, https://doi.org/10.1016/j.cej.2017.04.103.
[158] L. Dong, J. Liang, Y. Li, S. Hunang, Y. Wei, X. Bai, Z. Jin, M. Zhang, J. Qu, Effect of coexisting ions on Cr(VI) adsorption onto surfactant modified Auricularia auricula spent substrate in aqueous solution, Ecotoxicol. Environ. Saf. 166 (2018) 390–400, https://doi.org/10.1016/j.ecoenv.2018.09.097.
[159] Q. Yang, Y. Wang, J.J. Wang, F. Liu, N. Hu, H. Pei, W. Yang, Z. Li, Y. Suo, J. J. Wang, High effective adsorption/removal of illegal food dyes from contaminated aqueous solution by Zr-MOFs (UiO-67), Food Chem. 254 (2018) 241–248, https://doi.org/10.1016/j.foodchem.2018.02.011.
[160] D. Balarak, F.K. Mostafapour, S.M. Lee, C. Jeon, Adsorption of bisphenol a using dried rice husk: Equilibrium, kinetic and thermodynamic studies, Appl. Chem. Eng. 30 (2019) 316–323, https://doi.org/10.14478/ace.2019.1013.
[161] D. Robati, B. Mirza, R. Ghazisaeidi, M. Rajabi, O. Moradi, I. Tyagi, S. Agarwal, V. K. Gupta, Adsorption behavior of methylene blue dye on nanocomposite multi-walled carbon nanotube functionalized thiol (MWCNT-SH) as new adsorbent, J. Mol. Liq. 216 (2016) 830–835, https://doi.org/10.1016/j.molliq.2016.02.004.
[162] M. Rajabi, B. Mirza, K. Mahanpoor, M. Mirjalili, F. Najafi, O. Moradi, H. Sadegh, R. Shahryari-ghoshekandi, M. Asif, I. Tyagi, S. Agarwal, V.K. Gupta, Adsorption of malachite green from aqueous solution by carboxylate group functionalized multi-walled carbon nanotubes: Determination of equilibrium and kinetics parameters, J. Ind. Eng. Chem. 34 (2016) 130–138, https://doi.org/10.1016/j.jiec.2015.11.001.
[163] A.H. Jawad, S.N. Surip, Upgrading low rank coal into mesoporous activated carbon via microwave process for methylene blue dye adsorption: Box Behnken Design and mechanism study, Diam. Relat. Mater. 127 (2022), https://doi.org/10.1016/j.diamond.2022.109199.
[164] Y. Chen, R. Shan, X. Sun, Adsorption of cadmium by magnesium-modified biochar at different pyrolysis temperatures, Bioresources 15 (2020) 767–786, https://doi.org/10.15376/biores.15.1.767-786.
[165] Y. Kuang, X. Zhang, S. Zhou, Adsorption of methylene blue in water onto activated carbon by surfactant modification, Water (Switzerland) 12 (2020) 1–19, https://doi.org/10.3390/w12020587.
[166] H. Zhu, X. Liu, Y. Jiang, D. Lin, K. Yang, Sorption kinetics of 1,3,5-trinitrobenzene to biochars produced at various temperatures, Biochar. 4 (2022), https://doi.org/10.1007/s42773-022-00157-y.
[167] J.O. Ojediran, A.O. Dada, S.O. Aniyi, R.O. David, Functionalized Zea Mays Cob (FZMC) as low-cost agrowaste for effective adsorption of malachite green dyes data set, Chem. Data Coll. 30 (2020) 100563, https://doi.org/10.1016/j.cdc.2020.100563.
[168] L. Azeez, A. Lateef, S.A. Adebisi, A.O. Oyedeji, Novel biosynthesized silver nanoparticles from cobweb as adsorbent for Rhodamine B: equilibrium isotherm, kinetic and thermodynamic studies, Appl. Water. Sci. 8 (2018) 1–12, https://doi.org/10.1007/s13201-018-0676-z.
[169] U.J. Etim, S.A. Umoren, U.M. Eduok, Coconut coir dust as a low cost adsorbent for the removal of cationic dye from aqueous solution, J. Saudi Chem. Soc. 20 (2016) S67–S76, https://doi.org/10.1016/j.jscs.2012.09.014.
[170] S. Shakoor, A. Nasar, Adsorptive treatment of hazardous methylene blue dye from artificially contaminated water using cucumis sativus peel waste as a low-cost adsorbent, Groundw. Sustain. Dev. 5 (2017) 152–159, https://doi.org/10.1016/j.gsd.2017.06.005.
[171] F. Mashkoor, A. Nasar, Preparation, characterization and adsorption studies of the chemically modified Luffa aegyptica peel as a potential adsorbent for the removal of malachite green from aqueous solution, J. Mol. Liq. 274 (2019) 315–327, https://doi.org/10.1016/j.molliq.2018.10.119.
[172] A.M. Aljeboree, A.F. Alkaim, Comparative removal of three textile dyes from aqueous solutions by adsorption : As a model (corn-cob source waste) of plants role in environmental enhancement, Plant Arch 19 (2019) 1613–1620.
[173] M.A. Ahmad, N. Ahmad, O.S. Bello, Adsorptive removal of malachite green dye using durian seed-based activated carbon, Water. Air. Soil. Pollut. 225 (2014) 1–18, https://doi.org/10.1007/s11270-014-2057-z.
[174] Z.A. Alo, L.D.W. Azreenie Nazlyeen Amjah, Ahmed Saud Abdulhameed, Ali H. Jawad, Activated carbon from noodles food waste via microwave-assisted KOH for optimized brilliant green dye removal, Biomass Conv. Bioref. (2023).
[175] A.H. Jawad, A. Saud Abdulhameed, L.D. Wilson, S.S.A. Syed-Hassan, Z. A. ALOthman, M. Rizwan Khan, High surface area and mesoporous activated carbon from KOH-activated dragon fruit peels for methylene blue dye adsorption: Optimization and mechanism study, Chin. J. Chem. Eng. 32 (2021) 281–290, https://doi.org/10.1016/j.cjche.2020.09.070.
[176] N. Sivarajasekar, B. Rajoo, Agriculture waste biomass valorisation for cationic dyes sequestration: a concise review, Agriculture Waste Biomass Valorisation for Cationic Dyes Sequestration : A Agriculture Waste Biomass Valorisation for Cationic Dyes Sequestration A 7 (2015) 737–748.
[177] A.O. Dada, F.A. Adekola, E.O. Odebunmi, A.A. Inyinbor, B.A. Akinyemi, I. D. Adesewa, Kinetics and thermodynamics of adsorption of Rhodamine B onto bentonite supported nanoscale zerovalent iron nanocomposite, J. Phys. Conf. Ser. (2019) 1299, https://doi.org/10.1088/1742-6596/1299/1/012106.
[178] A. Mohamed, M.M. Ghobara, M.K. Abdelmaksoud, G.G. Mohamed, Separation and Purification Technology a novel and highly efficient photocatalytic degradation of malachite green dye via surface modified polyacrylonitrile nanofibers /biogenic silica composite nano fibers, Sep. Purif. Technol. 210 (2019) 935–942, https://doi.org/10.1016/j.seppur.2018.09.014.
[179] D.S.P. Franco, D. Pinto, J. Georgin, M.S. Netto, E.L. Foletto, C. Manera, M. Godinho, L.F.O. Silva, G.L. Dotto, Conversion of Erythrina speciosa pods to porous adsorbent for Ibuprofen removal, J. Environ. Chem. Eng. 10 (2022) 108070, https://doi.org/10.1016/j.jece.2022.108070.
[180] M.A. Al-Ghouti, M.Y. Ashfaq, M. Khan, Z. Al Disi, D.A. Da'na, R. Shoshaa, State-of-the-art adsorption and adsorptive filtration based technologies for the removal of trace elements: A critical review, Sci. Total Environ. 895 (2023) 164854, https://doi.org/10.1016/j.scitotenv.2023.164854.
[181] O. Moradi, G. Sharma, Emerging novel polymeric adsorbents for removing dyes from wastewater: A comprehensive review and comparison with other adsorbents, Environ. Res. 201 (2021), https://doi.org/10.1016/j.envres.2021.111534.
[182] A.O. Dada, F.A. Adekola, E.O. Odebunmi, F.E. Dada, O.M. Bello, B.A. Akinyemi, O.S. Bello, O.G. Umukoro, Sustainable and low-cost Ocimum gratissimum for biosorption of indigo carmine dye: kinetics, isotherm, and thermodynamic studies, Int. J. Phytoremediation. (2020) 1524–1537, https://doi.org/10.1080/15226514.2020.1785389.